ELSEVIER

Coordination Chemistry Reviews 225 (2002) 123–158

COORDINATION CHEMISTRY REVIEWS

www.elsevier.com/locate/ccr

Molecular mechanics and molecular dynamics simulations of porphyrins, metalloporphyrins, heme proteins and cobalt corrinoids

Helder M. Marques [a,*], Kenneth L. Brown [b]

[a] *Molecular Sciences Institute, School of Chemistry, University of the Witwatersrand, PO Wits, Johannesburg 2050, South Africa*
[b] *Department of Chemistry and Biochemistry, Ohio University, Athens, OH 45701, USA*

Received 6 April 2001; received in revised form 3 July 2001; accepted 19 July 2001

Contents

Abstract . . . 124
1. Introduction . . . 124
1.1. Porphyrins, metalloporphyrins and hemoproteins . . . 124
1.2. The cobalt corrinoids . . . 125
2. Force fields and their parameterization . . . 127
2.1. Molecular mechanics methods—a brief summary . . . 127
2.2. Modeling porphyrins . . . 130
2.3. Modeling corrins . . . 131
3. Applications of molecular mechanics methods . . . 132
3.1. Structure predictions: porphyrins . . . 132
3.1.1. The non-planar distortion of porphyrins . . . 132
3.1.2. Metal complexes and ligand interactions . . . 136
3.1.3. Metal-free porphyrins and related compounds . . . 137
3.1.4. The best-fit metal ion in a porphyrin . . . 139
3.1.5. The change in spin state of Fe(II) . . . 139
3.1.6. *N*-substituted porphyrins . . . 140
3.1.7. Interaction with substrates . . . 140
3.1.8. Dimeric porphyrins . . . 140
3.1.9. Crystal structure effects . . . 140
3.1.10. 'Designer' porphyrins . . . 140
3.2. Structure predictions: cobalt corrinoids . . . 141
3.2.1. Alkylcobalamins . . . 141
3.2.2. The corrin side chains and homolysis of the Co–C bond . . . 142
3.2.3. Compounds that do not crystallize: Ado-13-epiCbl . . . 142
3.2.4. MM and directed synthesis: (α-ribo)AdoCbl . . . 143
3.3. MD simulations: hemes and hemoproteins . . . 143
3.3.1. Molecular dynamics simulations of hemes and hemoproteins . . . 144
3.3.2. Porphyrins and hemoprotein model compounds . . . 144
3.3.3. The microperoxidases . . . 145
3.3.4. Hemoglobin and myoglobin . . . 146
3.3.5. The peroxidases . . . 147
3.3.6. Cytochromes . . . 148
3.4. MD simulations: the solution structure of cobalt corrinoids . . . 150
4. Summary . . . 152
5. Nomenclature . . . 152
Acknowledgements . . . 153
References . . . 153

* Corresponding author. Tel.: +27-11-716-2303; fax: +27-11-339-7967.
E-mail addresses: hmarques@aurum.chem.wits.ac.za (H.M. Marques), brownk3@oak.cats.ohiou.edu (K.L. Brown).

0010-8545/02/$ - see front matter © 2002 Elsevier Science B.V. All rights reserved.
PII: S0010-8545(01)00411-8

Abstract

Molecular mechanics (force field) methods have become popular as an adjunct to traditional methods for the examination of molecular structure. In this review, attention is focused on the use of molecular mechanics (force field) and molecular dynamics methods for the modeling of the structure of porphyrins, metalloporphyrins and hemoproteins, and the cobalt corrinoids (derivatives of vitamin B_{12}). © 2002 Elsevier Science B.V. All rights reserved.

Keywords: Molecular mechanics; Molecular dynamics simulations; Porphyrins; Cobalamin; Vitamin B_{12}

1. Introduction

Investigations into the chemistry of the porphyrins and the corrins, two important classes of biological tetrapyrrole systems, have utilized a veritable armory of experimental techniques and methodologies drawn from the physical, chemical, mathematical and biological sciences. The advent of cheap computing power in the last 20 years—and the development of the academic and commercial software packages that make the methodology readily accessible—has made computational chemistry methods extremely useful adjuncts to traditional methods of exploring molecular structure. In this review, we reflect on the use of molecular mechanics (MM) or empirical force field methods for modeling the structures of the porphyrins and the corrins. Whilst covering the more important developments in the field, especially over the last 10 years, the aim of the review is not to be comprehensive, but to inform the interested reader of the strengths and limitations of these methods in the study of these compounds.

MM methods rely on an idea that has been in the literature for many years [1–4]. The central notion is that the conformation of molecules can be described reliably with a simple mathematical model that draws on the concepts of a classical (non-quantum mechanical) description of molecular structure [5,6]. The focus is on the motion of the nuclei, as the molecule is treated as a set of interacting atoms; the energy consequences of all possible pair-wise interactions between the constituent atoms describes a molecular potential energy hypersurface. Minima on this surface correspond to stable conformations of the molecule, and the overall minimum on the surface (the global minimum) corresponds to the most stable molecular conformation. Should all conformers be discovered, it would be possible to treat the system as an equilibrium mixture among them, governed by a Boltzmann distribution. In principle, it would also be possible to take into consideration the vibrational motion of molecules about each minimum on the potential-energy hypersurface, and the migration of molecules over the saddle points connecting two neighboring conformers. The feasibility of such a description drops off very rapidly with molecular complexity and for even relatively small molecules, only the discovery of *some* conformers is a viable goal at present.

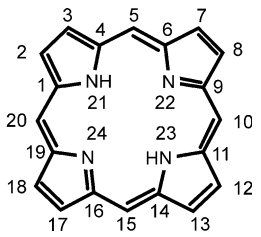

Fig. 1. Standard numbering scheme of the porphyrins. The carbon atoms at the 5, 10, 15 and 20 positions are referred to as the *meso* carbons. The C_α carbons are at 1, 4, 6, 9, 11, 14, 16 and 19. The C_β carbons are at 2, 3, 7, 8, 12, 13, 17 and 18.

1.1. Porphyrins, metalloporphyrins and hemoproteins

Porphyrins and their derivatives [7,8] play important and versatile roles in, inter alia, the transport and storage of dioxygen [9–11], in the activation of dioxygen towards reduction [12–14], in the oxidation of organic substrates [15–24], in the disproportionation of hydrogen peroxide [25–28], in bioenergetics (ranging from photosynthesis [29,30] to electron transport [31,32]), and in nitrite [33] and sulfite [34] reduction.

The basic porphyrin skeleton, together with the standard numbering scheme, is shown in Fig. 1. The fact that the porphyrin can play such diverse roles in biology is clear testimony of the effect its environment in the protein has on its properties. One of the most significant developments in porphyrin chemistry over the last 20 or so years has been the realization of the extraordinary flexibility of the porphyrin ring [35] which may be characterized by a combination of the six lowest frequency distortion modes (Fig. 2illustration see the Shelnutt web page at http://jasheln.unm.edu/jasheln/content/nsd_welcome.htm).

Among the most common distortions seen in porphyrins are the tilting of opposite pyrrole rings relative to each other which gives a saddled (*sad*) conformation and the twisting of the mean planes of opposite pyrrole rings relative to each other, which leads to the *meso* carbon atoms being alternately below and above the mean porphyrin plane (the so-called *ruf* conformation). The size of the porphyrin cavity is often approximated as the distance between the *trans* porphyrin N donors or twice the distance between an N donor and the centroid, Ct, of the mean porphyrin plane; a more

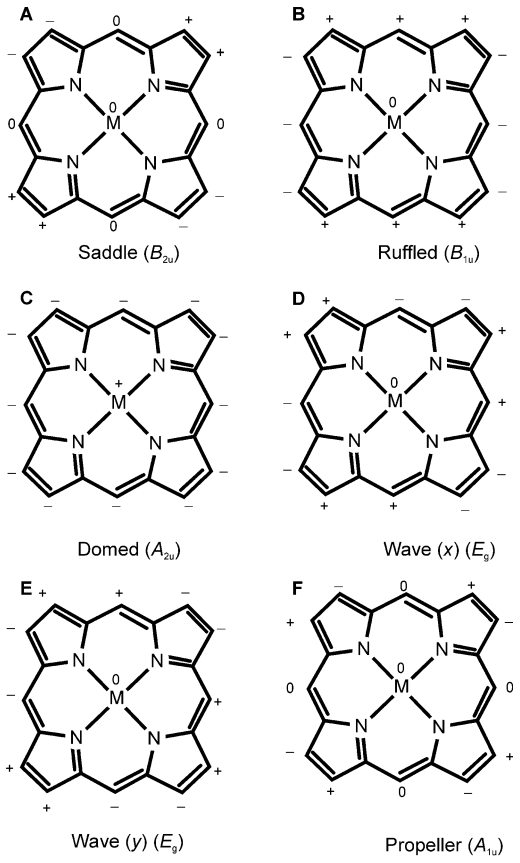

Fig. 2. The common distortion modes of the porphyrins, written in terms of the irreducible representations of a D_{4h} point group. In the saddled (*sad*) conformation, A, the metal ion and the *meso* carbon atoms are in or near the mean porphyrin plane (0) and the C_β atoms of the pyrrole rings are alternatively above (+) or below (−) the plane. In the ruffled (*ruf*) conformation, B, the planes of opposite pyrrole rings are twisted relative to each other. In the domed (*dom*) conformation, C, the metal rises above the mean porphyrin plane. Distortion D and E is called a wave (*wav*) distortion. A less common distortion mode is a propellering deformation F (*pro*) where two opposite pyrroles twist in opposite directions (when viewed along the N–Fe–N vector). Authors often refer to these porphyrin conformations by their point group. Thus the *sad* conformation is sometimes referred to as D_{2d}-*sad* and the *ruf* conformation as S_4-*ruf* (although the point group is actually D_{2d} as well). (For a dynamic . After Jentzen et al. [36].)

accurate measure is the length of the projection of the metal–nitrogen bond onto the mean plane of the pyrrole nitrogen atoms; thus, the core size is the radius of a cylinder through the porphyrin core with the nitrogens located on the cylinder's surface. It seems likely that this conformational flexibility is related to the properties and function of tetrapyrrole systems in such diverse systems as the hemoproteins [37–42], factor F_{430} from methyl-reductase [43,44], the photosynthetic antenna systems [45,46] and the photosynthetic reaction centers [47]; this proposition has recently been reviewed [48]. Several groups have explored the conformational flexibility of porphyrins by synthesizing porphyrins with a variety of peripheral substituents and investigating the effect of the crowding of the porphyrin periphery on its conformation [36,49–61]. Correlations between non-planarity and several optical spectroscopic parameters have been obtained for a number of porphyrins [50,62–64], and the relationships between structural parameters and the frequencies of several resonance Raman lines have been probed [63,65]. It has been suggested that the distortion of the porphyrin macrocycle can even control the spin state of Fe(III) [54,66].

1.2. The cobalt corrinoids

Based on the corrin macrocycle, the cobalt corrinoids are derived biosynthetically from uroporphyrinogen III [67–69], the porphyrin precursor, but lack the methine bridge between the A and D pyrrole rings. The macrocycle (Fig. 3) is substituted with seven methyl groups and seven amide side chains, including three acetamides (the *a*, *c* and *g* side chains) and three propionamides (the *b*, *d* and *e* side chains). The seventh side chain (the propionate *f* side chain at C17) is elaborated into the nucleotide loop, by esterification of an isopropanol, which is in turn esterified to the 3′ phosphate of a rare α-*N*-glycoside, α-ribazole-3′-phosphate, containing an unusual heterocyclic base, 5,6-dimethylbenzimidazole. This nucleotide provides a 'lower' or α axial ligand for the metal atom via coordination of the NB3 nitrogen (Fig. 3).

The complete Cbls are well known to undergo axial Bzm dissociation and protonation at NB3 (Fig. 3) to form the so-called base-off species. These base-off species have frequently been modeled by the nucleotide-free cobinamides (Cbis) [70–72], biosynthetic precursors of the Cbls [73,74] in which the axial nucleotide is missing, and the abiological 3,5,6-trimethylbenzimidazolylcobamides (Me_3BzmCbas) in which the Bzm coordinating nitrogen, NB3, is chemically methylated to prevent coordination [75,76].

Two organometallic species of cobalamins function as biological cofactors for enzymatic reactions. Methylcobalamin ($R = CH_3$ in Fig. 3) is a cofactor in methyl transfer reactions including the synthesis of methionine from homocysteine in some organisms [77–79] and in the CO_2 fixing pathway (the Wood–Ljungdahl pathway) in acetogenic organisms [80–84]. AdoCbl (so-called coenzyme B_{12}) however, is a coenzyme for a series of intriguing intramolecular 1,2-rearrangements [85], as well as for the reduction of ribonucleotides to deoxyribonucleotides in some organisms [86,87]. In each of these enzymatic reactions, catalysis is initiated by homolytic cleavage of the Co–C bond (the 'activation' of AdoCbl), a reaction which these enzymes cata-

lyze by some 10^9–10^{12} fold [88,89]. The mechanism(s) by which these enzymes achieve these extraordinary rate accelerations remain unknown and an important outstanding problem in bioinorganic chemistry.

It has recently become evident that the AdoCbl-dependent enzymes fall into three classes [90,91]. The mutases (methylmalonylCoA mutase, glutamate mutase, 2-methyleneglutarate mutase, and isobutyrylCoA mutase) catalyze carbon skeleton rearrangements, and constitute the class I enzymes. The eliminases (diol dehydratase, glycerol dehydratase, and ethanolamine ammonia-lyase) along with the ribonucleoside triphosphate reductases, a subset of the ribonucleotide reductases which catalyze the reduction of ribonucleotides to deoxyribonucleotides, constitute the class II enzymes. The less well studied aminomutases (such as lysine 5,6-aminomutase) catalyze 1,2-migrations of amino groups, require pyridoxal phosphate, and constitute the class III enzymes.

There are important differences between the class I and class II AdoCbl-dependent enzymes which suggests that the coenzyme may be activated for Co–C bond cleavage differently by these two classes of enzymes. ESR [92,93] and X-ray crystallographic studies [94–97] have shown that the class I mutases bind AdoCbl in a 'base-off' conformation, in which the α axial ligand position is occupied by the imidazole moiety of a histidine residue at the active site, while the uncoordinated nucleotide is buried in a hydrophobic pocket. This mode of Cbl binding was first discovered by X-ray crystallography for the association of CH_3Cbl with the Cbl binding domain of methionine synthase [98] and is associated with a conserved amino acid sequence including the coordinating histidine and a hydrogen bond relay network [99]. However, the class II enzymes are now known to bind AdoCbl in its 'base-on' conformation from ESR [100–102], sequence [103–106], and, more recently, X-ray crystallographic studies [107,108]. Another important difference between the class I and class II enzymes involves the specificity for the AdoCbl coenzyme. The class II enzymes accept many AdoCbl structural analogs as partially active coenzymes (al-

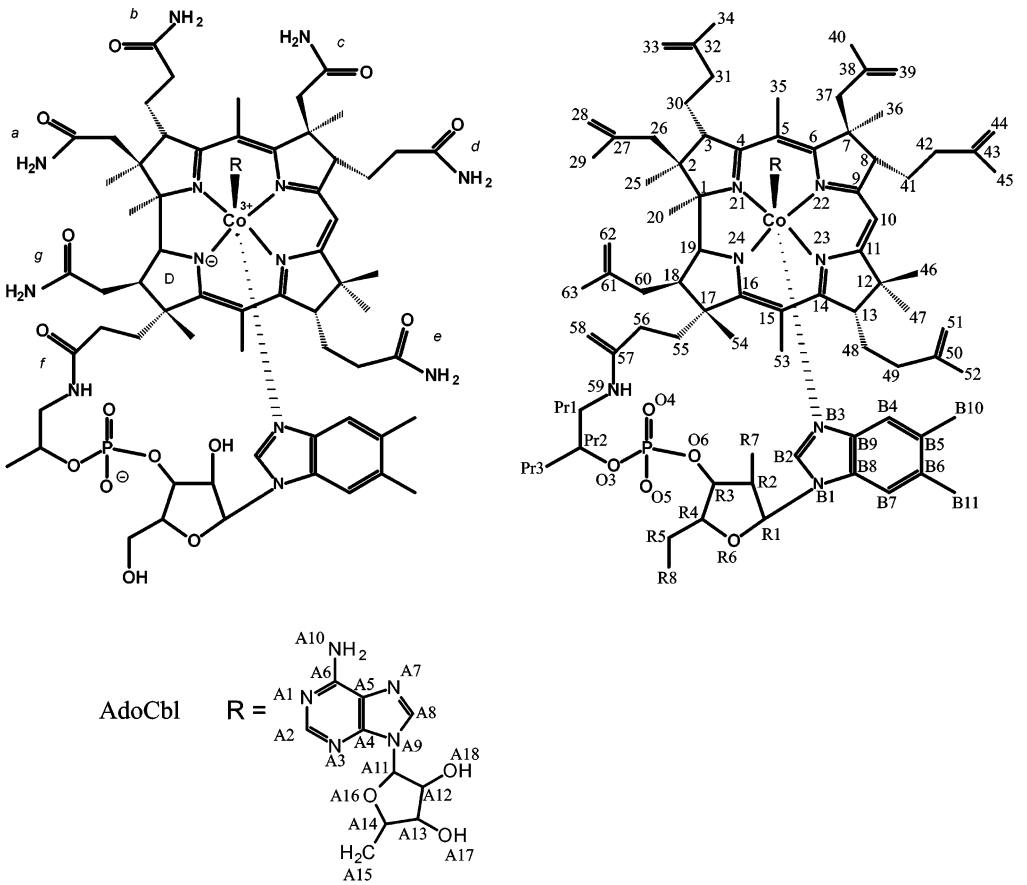

Fig. 3. Standard view of the cobalamins. The macrocycle corrin is adorned with three acetamide side chains that point towards the upper or β face of the corrin, and four propionamide side chains that point towards the lower or α face. The *f* side chain is elaborated into a nucleotide loop and a 5,6-dimethylbenzimidazole base coordinates the lower coordination site of Co(III). The standard numbering of the cobalt corrinoids is given in the diagram on the right. The quadrants with C5, C10, C15 and the C1–C19 bridge are referred to as the northern, eastern, southern and western quadrants, respectively. The species of known biochemical occurrence include cyanocobalamin (CNCbl, vitamin B_{12}, R = CN6), aquacobalamin (H_2OCbl^+, R = H_2O), and the two coenzymatically active species, methylcobalamin (CH_3Cbl, R = CH_3) and 5′-deoxyadenosylcobalamin (AdoCbl), commonly referred to as coenzyme B_{12}.

though others act as inhibitors) [109–111], while the class I glutamate mutase showed partial coenzymic activity with only one of 23 synthetically altered AdoCbl analogs investigated [112] (although naturally occurring AdoCbl analogs with uncoordinated axial nucleotides such as adenosyl-*p*-cresolylcobamide and pseudocoenzyme B_{12} are active as coenzymes [113]).

Since the original X-ray crystallography studies of Cbls by Hodgkin and Lenhert in the 1950s and 1960s [114–117], many crystal structures, including neutron diffraction studies of AdoCbl, have appeared [118–120]. In addition, the inner sphere coordination of free Cbls and their derivatives [121–125] and of the complexes of Cbls with proteins [126–128] have been studied by EXAFS, although interpretation of these results have sometimes been problematic, and some incorrect conclusions have been formed [124,128,129].

Within the past few years, X-ray crystal structures of B_{12}-dependent enzymes have begun to appear, including the B_{12}-binding domain of methionine synthase [98], methylmalonylCoA mutase [94–96], and diol dehydrase [107,108], and an NMR structure of the small B_{12}-binding subunit of glutamate mutase has also been reported [130]. Although this work has provided many structural details regarding the cobalamins and their enzymes, these revelations have not solved the problem of the mechanism of enzymatic activation of AdoCbl.

2. Force fields and their parameterization

2.1. Molecular mechanics methods—a brief summary

The use of MM models for performing calculations on organic molecules and, more recently, inorganic and bioinorganic complexes, has been reviewed in some detail [131–136], to which the interested reader is referred for a thorough treatment of the method and some of its more general applications in coordination chemistry. Only a very brief description is given here. Moreover, and specifically on the modeling of iron porphyrins by MM methods, the reader is directed to an excellent review that has appeared relatively recently [137].

A force field for MM calculations comprises a set of potential energy functions, which describe all bonded and nonbonded interactions between the atoms of a polyatomic molecule, and a set of parameters that provide numerical values for the constants in these functions. In a typical force field, the total energy of the molecule U_T (Eq. (1)) is the sum of the energy contributions from bond length deformation (U_B), bond angle deformation (U_θ), torsion angle deformation (U_ϕ), nonbonded interactions (U_{NB}), electrostatic interactions (either between bond dipoles or between point charges) (U_q), and out-of-plane deformations (U_{OOP}). In addition, cross terms to describe correlated motions such as stretch-bend and torsion-bend interactions are often included. These cross terms are essential for accurate calculations of rotational barriers and vibrational frequencies, particularly of organic molecules [138].

$$U_T = \sum_{i=1}^{m} U_B + \sum_{i=1}^{n} U_\theta + \sum_{i=1}^{p} U_{NB} + \sum_{i=1}^{r} U_q + \sum_{i=1}^{w} U_{\theta\,OOP} + \cdots \quad (1)$$

$$F = \frac{-\partial U}{\partial p} = k_p(p - p^0) \quad (2)$$

$$U = \frac{1}{2} k_p(p - p^0)^2 \quad (3)$$

Each of the summation terms in Eq. (1) adds a number of smaller energy contributions, the magnitudes of which are determined by how far the individual bonds, angles, torsions, etc., deviate from their 'ideal' or strain-free values. Thus, each structural parameter p has an ideal or strain-free value, p^0, such that when the observed value $p = p^0$, $U_p = 0$. The deformation of p away from p^0 is resisted by a restoring force (Eq. (2)), where k_p is the force constant. Integration gives the potential energy (Eq. (3)). Harmonic potentials (or variations thereof) are often used for the first two terms of Eq. (1) and the other terms are usually treated by special methods.

Some force fields have been developed, tested, and refined over many years, and the results produced with them are usually reliable. Notable among these are the force fields of Allinger and co-workers [139–144] developed for organic compounds, and those of Jorgensen and associates [145,146], Kollman and co-workers [147–149], and Karplus and co-workers [150], for modeling of biological macromolecules.

Molecular modeling seeks to rationalize a given set of experimental observations and (perhaps more interestingly) to predict molecular properties. Since the MM approach is interpolative by nature, the model can only be used within the limit of the set of observations utilized in its derivation and the user has to beware of extrapolating beyond the confines of the set of observations used in deriving the model. The results from unwarranted extrapolations are unlikely to be dependable. Often a user would want to utilize a force field to predict the structure of a novel compound. At least two conditions have to be satisfied: the novel compound must be appropriate for the force field; and the force field must be reliable. The types of novel compounds that can be meaningfully explored will be circumscribed by the way the force field was developed. A truly 'universal' force field should give reliable results for virtually any compound, but a force field designed for a specific class of compounds will be unlikely to give

useful results for a compound outside that class. A reliable force field requires thorough evaluation. Obviously, it must reproduce the experimental observations upon which its derivation was based and the predictions made using the force field must make chemical sense; but perhaps the most convincing way to demonstrate its reliability is to use the force field to predict structures not used in its derivation, or to predict novel structures, and then demonstrate the validity of the predictions by a subsequent structure determination.

MM methods have been extended to metal-containing systems only relatively recently. The task is not simple as there are many different kinds of atoms, and many have a variable coordination number, coordination geometry, oxidation state and spin state. Moreover, the influence of the open shell of *d* electrons on the structure of the compounds cannot be underestimated. As might be anticipated, a number of approaches have emerged. In some treatments, it is recognized that many of the constituents in a coordination compound are organic moieties. These portions of the molecule are then dealt with using a standard MM force field for modeling organic molecules. The parameter set is extended to account for the metal ion and its interactions with the other atoms in the molecule; such methods may therefore be termed *parameter extension force field methods*. The M–L (L = ligand) bond is treated as a covalent bond, and is defined by an ideal bond length with an appropriate force constant; similarly, L–M–L is treated as a standard valence bond also with an ideal angle and a corresponding force constant. This approach is one way of circumventing a major problem that has to be faced when modeling systems containing metal ions, namely the derivation of electrostatic parameters for the M–L bonds. There is often an uncertainty in the appropriate choice of dielectric constant [151–153] and in calculating the partial charges on the metal and the donor atoms [154–156]. Whilst there are some procedures for partitioning charges [157–161], there is as yet no agreement on methods for determining M–L dipole moments. In many cases, M–L dipole moments are neglected altogether [63,162–166] and in essence they are subsumed into the M–L bond stretching and L–M–L angle bending terms.

Another approach treats the metal–ligand interaction by a 'points-on-a-sphere' model, reminiscent of the VSEPR model widely used in inorganic chemistry for predicting the shapes of molecules. Although the metal–ligand interaction has an ideal bond length, instead of defining bond angles, a Urey–Bradley approach is used [167], in which 1,3-van der Waals interactions (usually not taken into account and assimilated into the angle bending term) between the ligand donor atoms bonded to the metal ion are used to model the coordination sphere. Naturally, electrostatic parameters are much more critical in this approach.

The participation of metal *s* and *d* electrons in bonding in coordination compounds makes the MM modeling of metal-containing system difficult. If one is to avoid having to develop parameters for each spin state, coordination number and oxidation state for each metal in each class of compounds (as has been proposed, for example, for Fe in the iron porphyrins [165]), then special potential functions are required [168]. Such force fields may be termed *universal* or *generalized force fields*. They have been developed to model as wide a range of metal-containing compounds as possible. Examples are the Universal Force Field (UFF) of Rappé and co-workers [169] (recently employed, for example, for the modeling of the cobalt corrinoids [170]), the MOMEC force field of Comba and Hambley [171], the SHAPES force field of Allured, Kelley and Landis [172], and the Ligand Field Molecular Mechanics (LFMM) force field of Deeth [173]. Whilst generalized force fields are obviously attractive for their very generality, it must be accepted that generality may come at the expense of quality and that such force fields may not produce results that are as good as those obtained from those with a parameter set specifically developed for molecules of a particular class.

Recently, Schweitzer-Stenner and co-workers reported an interesting new approach to MM calculations [174]. In their approach, the molecule is subdivided into local units, each made up of an atom and its nearest neighbors. The potential function of each local unit is assumed to depend only on the position of the atoms in that unit; the vibrational force field is then expressed as the sum over the contributions from all units. Since local units usually display high local symmetry because the bonds formed and their spatial disposition are necessarily dictated by the valence and hybridization state of the atom, the number of possible interaction parameters is limited. Ab initio results are used to show that the internal force constants of each local unit are transferable to other molecules; hence it becomes possible to calculate the internal force constants of each local unit from small molecules, and to use these to build up the potential function of large molecules such as porphyrins. The authors show that this approach reproduces rather well the vibrational frequencies and mode compositions of molecules such as porphyrins with a 40–80% reduction in the number of force field parameters. Whether this approach will be useful in answering any of the number of questions that have been asked of and answered by more common force field methods remains to be seen. Initial results are very promising; for example with the approach reproducing the structure and normal modes of vibration of several very ruffled Ni(II) porphyrins [175].

Whatever approach is adopted, the transferability of force field parameters remains—and probably will always remain—a major problem with MM modeling of

transition metal complexes [168]. Perhaps in recognition of this, an approach that is currently gaining momentum is to incorporate both quantum mechanical (QM) and molecular mechanical modeling of the molecule, with the QM modeling focused on the metal ion, and the MM modeling on the rest of the molecule [176,177]. Using such an approach it should be possible in principle to develop truly universal force fields for metal-containing systems, and moreover to examine systems which involve a fundamental rearrangement in the electronic distribution as would occur, for example, on a change of spin state or oxidation state of the metal ion, or if chemicals are made or broken [177]; or where electronic effects such as polarization are likely to be important [178]. The methodology is still very much in the development stage, and a number of issues such as how to treat the QM/MM boundary, the size of the QM-treated region on the overall results, and the effect of long-range interactions on the electron distribution in the QM region, still have to be addressed [178].

Pertinent to the subject matter of this review, the corrin core of CNCbl has been modeled [179] using the INDO/1 procedure while the peripheral substituents were modeled using MM methods (Tripos Force Field [180], Tripos Associates, St. Louis, MO); the approach adopted allows for charge transfer between the quantum mechanically and classically treated fragments and gives a structure that is in good agreement with that determined in the solid state [181].

Maseras [182] performed QM/MM calculations with a program constructed from GAUSSIAN 92/DFT [183] for the QM calculations and MM3(92) [143] for the MM part on picket-fence porphyrin dioxygen complex Fe(T_{piv}PP)(1-MeHIm)(O_2). The modeled structure agreed well with the X-ray structure. By comparing the results with a porphyrin lacking the picket-fence arms, it was shown that the amide groups of the picket-fence stabilize the dioxygen complex by some 20 kJ mol^{-1} because of an O···H(N) interaction. The same group [184] have recently extended their investigations to the 4-coordinate Fe(porphine) system, the 5-coordinate Fe(HIm)(porphine) system, and 6-coordinate Fe(HIm)(O_2)(porphine). Structural parameters from the parts of the molecule modeled by QM methods are generally in good agreement with the experimental observations, but discrepancies from the MM-modeled portions can be quite large since the authors have used the default MM3 parameters rather than the parameters that have been developed by other groups specifically for modeling porphyrins with the Allinger force field.

The aim of MM methods is to find minima on the potential energy hypersurface, corresponding to situations where the forces on each atom are balanced. Various algorithms are available for searching conformational space for these stationary points [185,186]. Among the most commonly used are the steepest descent, conjugate gradient and the Newton–Raphson block diagonal methods, although a combination of these may be employed; thus, a conjugate algorithm may be switched to a Newton–Raphson procedure as convergence approaches, since the latter tends to converge faster near the convergence point. These minimization algorithms often locate local energy minima on the potential energy surface. It is therefore necessary to adopt other procedures to search conformational space more effectively. Even so, since the number of stable conformations increases rapidly with molecular complexity, it is virtually an impossible task to find all conformations, and one is usually left with no option but to sample conformational space.

Search procedures include exhaustive grid search methods, in which, for example, every single rotatable bond is rotated through a full 360° in some step increment. The method is clearly restricted to only the very smallest molecules and even amongst these, often only to rotations about a single bond or a limited number of bonds if there is reason to believe that the molecular structure is particularly sensitive to rotations about such bonds. Very different in their philosophy are random search methods. In these procedures the current structure is saved, randomly changed, and then fully energy-minimized. By repeating the procedure many times, it is hoped that a significant portion of conformational space, and certainly conformational space near an energy minimum discovered by some other procedure, can be explored. Examples of this approach include the RIPS (random incremental pulse search) algorithm [187] and the Metropolis Monte Carlo algorithm [188].

Molecular dynamics methods [189] seek to reproduce the dynamic behavior of molecular systems by describing the change in position of the atoms with time. The future positions and velocities of atoms are predicted based on their current positions and velocities by solving the classical equations of motion. The first quantity evaluated is the force acting on each atom (the negative gradient of the potential energy); the acceleration is then evaluated by dividing by the mass. The change in velocity of each atom is the integral of the acceleration, and the change in position of each atom is the integral of the velocity. The leapfrog algorithm [190] is often used to solve these equations. The extent of the motion can be controlled by varying the temperature at which the simulation is performed. It is quite common to perform simulations by first heating the molecule from a low temperature to an artificially high temperature (between 600 and 1000 K is common), and then performing the run phase of the simulation at this temperature. The high temperatures facilitate the surmounting of potential energy barriers. Samples are taken at random or fixed intervals, fully energy-minimized, com-

pared and sorted; new conformations are stored. This procedure is sometimes referred to as a quenched dynamics simulation. Alternatively, after the run phase the system is slowly cooled, and finally fully energy-minimized; this is a simulated annealing (SA) procedure [191]. Experimental information may be incorporated into an MD simulation as a set of restraints, thus limiting the extent of conformational space that has to be searched to those regions that satisfy the experimental observations. An example of this is the adding of dummy bonds between protons to restrain (usually with simple parabolic functions) the proton–proton distance at values commensurate with nOe strengths obtained from 2D NMR experiments [192,193].

2.2. Modeling porphyrins

Standard force fields originally developed for investigating the structure of organic compounds have been profitably applied to investigating the structure of metal free porphyrins and related compounds. Thus, Bruice and co-workers [194,195] used MM and quenched molecular dynamics simulations at 600 K with the CHARMm force field [150] to explore the structure of bridged metal-free cofacial tetraphenylporphyrin dimers. Vergeldt and co-workers [196] used the same force field, together with a distance-dependent dielectric constant to simulate the screening effect of solvent water, to explore the structure of metal-free tetrakis(*N*-methylpyridyl) porphyrins. Connolly's group [197] used the version of the MM2 force field [142] known as MM+ in the HYPERCHEM suite of programs (Hypercube Inc., Gainesville, FL) to explore the structure of a number of *meso* tetra-alkyl and tetra-aryl porphyrins, and to correlate the structure with their photophysical and redox properties. Others have used MM+ for similar purposes; Trull and co-workers [198] investigated the structure of a series of nitrobenzyl mono- and diesters of *meso*-porphyrin, whilst Lament et al. [199] used it to explore the structure of rosarin, a nonaromatic hexapyrrolic expanded porphyrin. Battersby and co-workers [200,201] have used the MM2 force field to investigate the structure of potential intermediates in the biosynthesis of uroporphyrinogen III. Bonar–Law and Sanders [202] used both MM2 and the AMBER force field [147] to explore the structure of porphyrins capped by a cyclic dilactone of cholic acid. Casiraghi and his group have used the CVFF force field [203] (Biosym Technologies, San Diego, CA) to explore the structure of *meso*-glycosylated porphyrins [204]. Ravikanth [205–208] used the AMBER force field to study the structure of a series of novel 'basket-handle' porphyrins (porphyrins containing a short chain of variable length either across or along the porphyrin periphery). The SYBYL force field [180] has been used to investigate the structure of compounds based on a substituted protoporphyrin IX nucleus [209].

One of the first attempts to model metalloporphyrins was by Abraham and co-workers [210] who used the program MODELS [211] augmented with non-bonded potentials for H, C, N and O [212,213] to investigate the structure of a number of Co(III) porphyrins bis-ligated with pyridine, 1-methylimidazole, 4-methylpiperidine and isoquinoline. The program allowed for the relaxation of a limited number of structural parameters, and both the porphyrin and the planar aromatic ligands were treated as rigid, planar structures. Electrostatic contributions to the energy were obtained from partial atomic charges, apportioned using the CHARGE3 program [214].

A number of groups have extended the parameter set of standard MM force fields to study metalloporphyrins. For example, Angelucci et al. [215] extended the CVFF force field, whilst Scott [216] modified some bond stretching, angle bending and torsional parameters of the standard MM2 force field [140,141] and added parameters for Ni(II) to investigate the structure of F_{430}, the Ni-containing cofactor of *S*-methyl coenzyme M reductase enzyme of methanogenic bacteria.

Munro and co-workers [162] used a modified version of Allinger's MM2(87) [140,141] force field to analyze the factors that affected metalloporphyrin conformations. All M–L bonds were treated by a bonded formalism, with all dipoles involving the metal ion set to zero. The standard MM2 dipole parameters were retained for the porphyrin, as were the SCF B-MO calculations for the extended delocalized B electron system. The force field parameters for all interactions not involving the metal ion were the default MM2 parameters; those for potentials involving the metal ion were developed by attempting to reproduce as accurately as possible the crystal structures of six porphyrins, with cations of very different sizes (P(V), $S=0$ Ni(II), $S=1$ Fe(II), Zn(II) and Pb(II)), and hence porphyrin cores showing a very wide range of ruffling. In addition, ten imidazole ferric porphyrin complexes were used to derive parameters for low spin Fe(III). Factors investigated included (i) the effect of the size of the metal ion coordinated by the porphyrin on the structure of the porphyrin core; (ii) the effect of the orientation of planar axial ligands on the porphyrin core; and (iii) the effect of the orientation of *meso*-phenyl substituents on the structure of TPP derivatives. We shall refer to this force field as the Munro force field [162,164,165].

In a remarkable sustained effort, Shelnutt and co-workers have made extensive use of MM calculations to probe the effect of peripheral substituents of the porphyrin ring on the conformation of the porphyrin core. Their force field, which we shall refer to as the Shelnutt force field [63], is based on a normal coordinate analysis of NiOEP [217–219] and the crystal structure of NiOEP [220], from which parameters for the

DREIDING force field [221] were determined. They usually ignore electrostatic contributions to the strain energy, as they found that inclusion of partial charges had no significant effect on the calculated structures [222]. However, the inclusion of partial charges and the use of the softer exponential-6 potential for H atoms instead of the Lennard–Jones 12-6 potential of the DREIDING force field gives more accurate relative conformational energies [223,224].

The UFF force field of Rappé and co-workers [169] has been used to investigate the structure of possible intermediates in the P450 catalytic cycle [225]. Pispisa and colleagues ([226] and references therein) have developed their own MM program, and the interested reader is referred to the original papers for a fuller description. The program uses a potential function similar to that of MM2 [140] and a minimization algorithm based on the rotational isomeric state model of Mattice and Suter [227]. The program has been used to explore the structure of protoporphyrin–polypeptide–naphthalene compounds, and to rationalize the observed photophysics of these systems.

2.3. Modeling corrins

The potential functions and formalism of the MM2 force field [140,141] together with a parameter set derived specifically to reproduce the solid state structures of the cobalt corrinoids [228,229], have been used to explore the structure of these molecules. The non-bonded parameters used for Co(III) were similar to those used for Fe(III) in the modeling of the iron porphyrins [162,164–166] and not dissimilar to those used in the UFF [169]. The MM2 van der Waals parameters were used for all other atoms. A survey was conducted of appropriate corrin structures deposited in the Cambridge Structural Database (CSD) and the mean values of the bond lengths, bond angles and dihedral angles was determined [228]. Atoms were then divided into classes, and the mean and standard deviation of class-equivalent bond lengths and bond angles was found. Differences between classes were checked for statistical significance and the number of classes was reduced as far as possible. The metal–ligand interaction was treated within a covalent-bonded formalism, with bond dipole moments set to zero.

The derivation of the force field parameters was done by initially setting the strain-free values of the bond lengths and bond angles to the crystallographically observed mean values and setting the initial values of the force constants to those used in MM2 [139,140] for analogous situations, the Munro force field [162,166], or parameters used by a number of investigators for the modeling of a variety of Co(III) compounds [131,230–240]. The crystal structure of CNCbl [241] was used as the test structure. After each energy minimization, a random number generator was used to change the coordinates of every atom to check conformational space in the neighborhood of the converged structure. The values of the structural parameters obtained were compared with the values from the statistical survey, and the force field parameters were adjusted on a trial-and-error basis until an acceptable fit to the average crystallographic values was obtained. With the final force field parameters [228], the bond lengths, bond angles and dihedrals were reproduced with root mean square differences (r.m.s.d.) of 0.01 Å, 2.4° and 4.2°, respectively, of the crystallographic means; this is well within their experimental standard deviations, and within the accepted criteria for a good fit [169,228,242].

More recently [229], the force field has been re-developed for use by codes such as MM+ which utilize a Urey–Bradley formalism (1,3-van der Waals interactions are used to model the coordination sphere of a metal ion) rather than the more traditional formalism of MM2 where L–M–L′ angles and L–L′–M–L′ torsions are handled like any other angles and torsions. The results from the two approaches are comparable.

It must be appreciated that approaches such as this will at best reproduce an *average* cobalt corrin structure. If a direct comparison is made between such a structure and the solid state structure of any specific cobalamin, differences will almost invariably be found, especially in the more flexible parts of the molecule. Moreover, such MM simulations are often performed on the isolated molecule, so the influence of the environment, be it the solid state, or the solvent, may well have an effect on the structure. A comparison between some modeled structures and the corresponding crystal structure is shown in Fig. 4.

The validity of the force field has been thoroughly assessed. As mentioned (see above), the crystal structures used to develop the force field were satisfactorily reproduced. The force field was used to predict the structure of cyano-13-epicobalamin, where the *e* side chain at C13 has been epimerized from the lower to the upper face of the corrin ring. The structure predicted by the force field [228] was very similar to the known crystal structure [243] which had not been used during the derivation of the force field; the validity of the predicted structure was confirmed when a new determination of the structure was carried out [244]. Epimerization of the *d* side chain at C8 of CNCbl leads to cyano-8-epicobalamin, the structure of which was unknown at that stage; this was therefore predicted by MM methods. The compound was subsequently prepared, crystallized and the structure determined by X-ray diffraction [245]. Again, a very satisfactory agreement was found between the observed and the predicted structure (Fig. 5).

An alternative way of testing a force field's validity is to verify other experimental observations. For example,

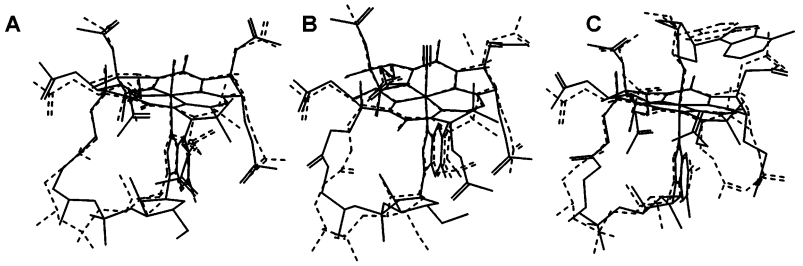

Fig. 4. An overlay of MM-modeled structures of A: CH_3Cbl, B: CNCbl, and C: AdoCbl (solid line) and the corresponding crystal structures (broken line). The modeled structures are consensus structures from MD/SA calculations (see text).

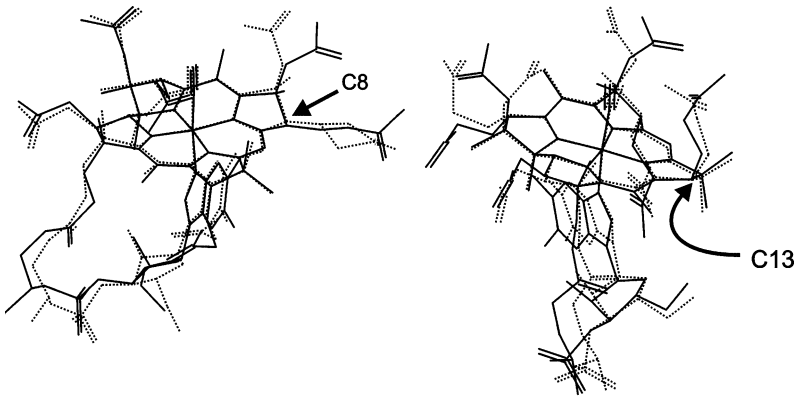

Fig. 5. A comparison of the MM prediction of the structures of cyanocobalamins epimerized at C8 and C13 (solid lines) compared to the crystal structures (broken lines).

cross-peaks in the 2D NMR spectrum of AdoCbl had been observed [246] which were inconsistent with the orientation of the adenosyl ligand observed in the solid state, where the adenine ring system, virtually parallel to the corrin ring, is over the southern quadrant (Fig. 6) of the molecule when viewed from above [120]. A two-state model was proposed [246] in which the Ado ligand flips between the southern conformation and an eastern conformation in which the Ado ligand has been rotated by some 50° in a counterclockwise direction. The strain energy profile for rotating the Ado ligand by a full 360° relative to the corrin ring was determined by MM methods and four energy minima were found (Fig. 7). The global minimum finds the Ado ligand in the southern conformation; surmounting a small energy barrier leads to the eastern conformation. Two larger barriers lead to the northern conformation and to the western conformation, respectively. Thus, the population of both a southern and an eastern conformation by AdoCbl in solution at room temperature appears very feasible indeed. It was subsequently shown [247] that at 60 °C the northern and western conformations are also visited by AdoCbl in solution.

Finke and co-workers [170] have used MM and the UFF [169] to model the structures of MeCbl, AdoCbl, *R*- and *S*-DHPrCbl and AdePrCbl, and found the results comparable to those reported by Marques and Brown using MM2 [228].

3. Applications of molecular mechanics methods

3.1. Structure predictions: porphyrins

3.1.1. The non-planar distortion of porphyrins

Munro et al.'s parameterization of the MM2(87) force field for metalloporphyrins [152,164,165] yielded a force field that was able to quite accurately reproduce the moderate non-planar distortion in a number of

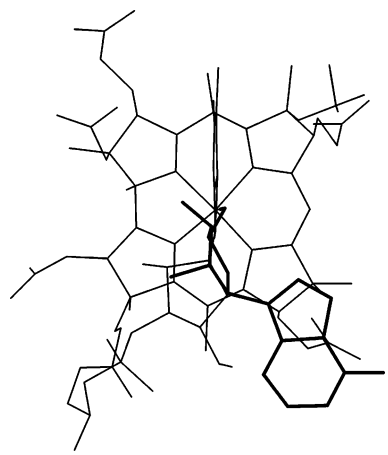

Fig. 6. The solid state structure of AdoCbl [120]. The 5′-deoxyadenosyl ligand is positioned over the southern quadrant of the molecule, overlaying ring C.

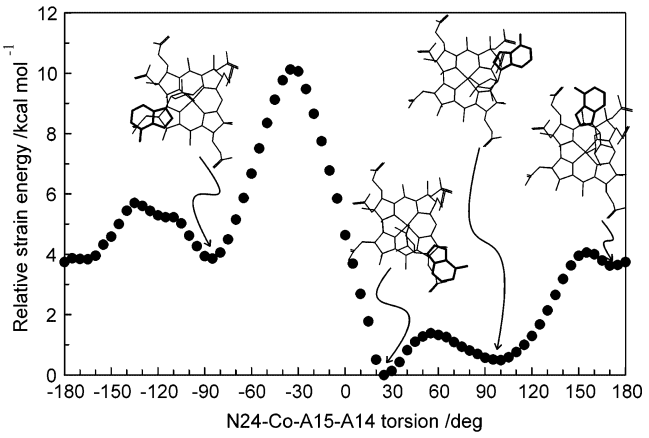

Fig. 7. The strain energy profile for rotation of the adenosyl ligand relative to the corrin ring. The four minimum energy conformations found (from left to right) are referred to as the western, southern, eastern and northern conformations, respectively. The southern conformation is similar to the conformation found in the solid state (see Fig. 6).

porphyrins (Fig. 8) by merely varying the equilibrium M–N bond length and the stretching force constant. However, to adequately model the severe out-of-plane distortion in a porphyrin such as $[P(TPP)(OH)_2]^+$, which contains very small P(V), or a domed porphyrin such as [Pb(TPrP)], which contains very large Pb(II), required modification of torsions involving the metal ion and the porphyrin ring and, in the case of Pb(II), a change in the equilibrium N–Pb–N bond angle to described what is essentially a square pyramidal structure. The size of the metal ion is clearly an important factor in determining the extent of porphyrin non-planar distortion. Thus, the P(V) complex is in a severe *ruf* (i.e. S_4) conformation; the complexes of $S=0$ low spin Ni(II) are either ruffled or planar; the $S=1$ Fe(II) complex is moderately ruffled; Zn(II) is planar; and Pb(II) is domed (C_{2v}). Some differences between crystallographically observed and modeled C–C bond lengths (up to 0.05 Å) in the porphyrin core were attributed to the application of the standard MM2(87) heterocycle force constants and the SCF MO treatment of less complex B-electron systems to the tetrapyrrole system of the metalloporphyrins.

The preponderance of a *sad* core geometry in [M(TPP)] complexes has been noted [35]. An MM investigation [162] subsequently showed that significant *sad* ruffling of the porphyrin core occurs when at least one of the phenyl dihedral angles is $< 55°$, since such a conformation minimizes the repulsive non-bonded interactions between the tilted phenyl substituents and the porphyrin pyrrolic units. A careful evaluation of the energy differences between planar, *sad* and *ruf* conformations has shown that, at least for modest distortions from planarity, these conformations are all close in energy. This suggests that, particularly in highly substituted porphyrins, core deformation is an efficient stereochemical response to steric crowding. It should be noted, however, that the porphyrin moiety is sufficiently pliable that even in the case of a highly substituted porphyrin such as H_2DAP, out-of-plane distortion is not the only mechanism available for steric strain relief. Thus [248], an X-ray crystallographic investigation of the structure of H_2DAP shows it to be planar with an elongation along the 5,15 axis.

Although the extension to the MM2(87) force field developed by Munro and co-workers [162] reproduced M–N and C–C–C, C–N–C and N–C–C angles rather well (to within 0.01 Å and 2°, respectively), C–C and C–N bond lengths were not well reproduced, often differing by as much as 0.07 Å from the crystallographically observed values. The reason was traced to the SCF B-electron MO calculations that are part of the MM2(87) force field for delocalized electron systems. In a revision of the MM2(87) force field parameters for porphyrins, the same group [165] conducted a thorough statistical survey of iron porphyrins available at that time in the CSD (120 structures), and used the mean crystallographic values for the strain-free bond lengths for bonds in the porphyrin core, abandoning the SCF MO calculations entirely. The force field parameters were then refined by modeling two structures each of penta- and hexa-coordinate high- and low-spin ferrous and ferric porphyrins, intermediate spin ($S=1$) penta- and hexa-coordinate ferric porphyrins, and intermediate spin tetra-coordinate ferric porphyrins. With these

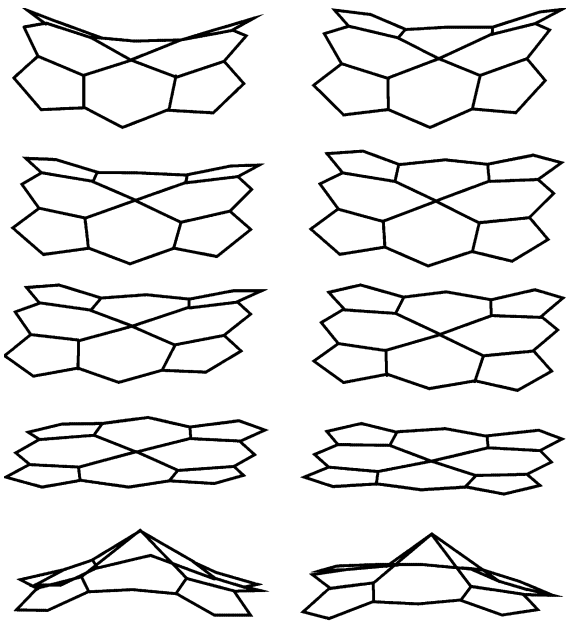

Fig. 8. A comparison of the crystallographic (left) and the MM energy-minimized structures obtained by a modified version of MM2(87) with parameters for modeling metalloporphyrins (right). The central ion from top to bottom is P(V), $S=0$ Ni(II), $S=1$ Fe(II), Zn(II) and Pb(II). See Ref. [162] for references to the crystal structures.

revised parameters, all bond lengths were reproduced to better than 0.015 Å, and angles and torsions to better than 1.5 and 4°, respectively. The force field was then used to examine the structure of [FeTPP] using quenched dynamics techniques and the algorithm of Gerber et al. for ring systems [249]. Both the planar and the S_4 ruffled core of [FeTPP] were discovered, with the planar conformation only very marginally more stable (by 0.03 kcal mol^{-1}) than the ruffled conformation.

A further refinement to these force field parameters was made specifically for the modeling of six-coordinate low-spin imidazole and pyridine complexes of ferric porphyrins [164]. Bond lengths of four ferric tetramesityl porphyrin complexes containing either pyridine or imidazole as axial ligands, including the exceptionally ruffled $[Fe(TMP)(1,2\text{-}Me_2Im)_2]^+$ complex, were reproduced to better than 0.010 Å; bond angles were reproduced to better than 0.5°; and torsional angles to better than 2°. This study showed, inter alia, that the occurrence of the *ruf* conformation of the porphyrin core in six coordinate complexes hinges on the relative perpendicular orientation of the axial ligands, and confirmed that the *sad* conformation in ferric *meso*-tetraaryl porphyrins is primarily determined by the steric interaction between the *meso* aryl substituents and the porphyrin core. However, Walker and co-workers [250], who used the same force field to investigate the structure of $[Fe(TPP)(4\text{-}CNPy)_2]^+$, argue that there is an electronic effect as well in controlling the ruffling. The origin is likely to be the partial delocalization of d_{xy} unpaired electron spin into the $\alpha_{2u}(\pi)$ porphyrin orbital, which is made possible by the twisting of the nitrogen p_z out of the mean porphyrin plane, attendant on S_4 ruffling of the porphyrin core.

The response of a porphyrin to steric crowding has been extensively explored in the work of Shelnutt and colleagues. They began a long and impressive study of the structure of metalloporphyrins in which MM methods have played an important role by validating the force field calculations against the known structure of highly ruffled NiOPTPP [220]. Good agreement was found, with the force field somewhat overestimating the degree of non-planar distortion of the porphyrin. (However, the standard DREIDING force field was unable to correctly predict the structure of a highly substituted free base porphyrin, DPP [251].) They then examined the structure of Ni(II) porphine, NiOEP, NiTPP, and a series of Ni(II) octaalkyl(aryl)tetraphenylporphyrins (NiOMTPP; NiOETPP; NiEPTPP; $NiTC_5TPP$; $NiTC_6TPP$; $NiTC_7TPP$; NiDPP) and found that out-of-plane distortion of a porphyrin in response to the steric pressure of the substituents on its periphery causes the core size to decrease. NiOMTPP, NiOETPP, NiOPTPP, NiDPP, $NiTC_6TPP$ and $NiTC_7TPP$ all adopt a *sad* conformation, whereas $NiTC_5TPP$ is predicted to be planar. Some of these results have been verified subsequently by crystallography. For example, $CuTC_5TPP$ is planar whereas NiOETPP, NiOPTPP and $NiTC_6TPP$ all have a *sad* conformation [252]. When it was demonstrated that the force field was capable of reproducing even subtle features of porphyrin structures, such as the decrease in core size with an increase in non-planar distortion, these workers could then investigate the relationship between core size and the frequency of the structure-sensitive resonance Raman lines. More recent MM calculations on [NiTPP] [253] indicate that the lowest energy conformation is a *ruf* conformation, and the *sad* and planar conformations are 1.70 and 1.78 kcal mol^{-1} higher in energy, respectively.

The reasons why some peripheral substituents favor a *ruf* conformation whereas others favor a *sad* conformation were explored [251]. X-ray crystallography shows that DPP exists in a very non-planar *sad* conformation, whereas $NiTC_5TPtP$ exists as a very non-planar *ruf* conformer. These observations are in good agreement with the calculated structures of NiDPP and $NiTC_5TPtP$ (the DREIDING force field produced an unrealistic structure for the free base DPP itself). The similarity of the X-ray structure of DPP and the calculated structure of NiDPP confirms that the ruffling of the porphyrins is a consequence of the steric interactions between the peripheral substituents, although the size of the metal ion does have an effect as well; thus, the Zn(II) analogs are calculated to be somewhat less ruffled than the Ni(II) complexes. *meso* Phenyl groups cause a porphyrin to undergo a *sad* deformation because of a steric clash between the phenyl substituent and the neighboring pyrrole rings. On the other hand, an alkyl substituent in the *meso* position favors a *ruf* conformation. The hydrogen atoms on the α carbon of the alkyl substituent force the alkyl group out of the plane; this moves the *meso* carbon out of the plane and triggers the *ruf* deformation. The difference in energy between planar NiDPP and the *sad* form was estimated to be 25 kcal mol^{-1}; that between planar and *ruf* $NiTC_5TPrP$ is 24 kcal mol^{-1}. Low temperature NMR studies demonstrate the preponderance of the ruffled conformations in solution. Calculations of the structure of $NiTC_5TMP$ and $NiTC_5TEP$ show these compounds to have a *ruf* conformation.

The structure of highly substituted octaalkyltetraphenylporphyrins has been investigated [254]. MM calculations show that M(II)OETPP remains sufficiently flexible to show a small, but significant, decrease in out-of-plane distortion as the size of M(II) increases; a result confirmed by crystallographic analysis. The identity of the metal ion was changed in the calculations by varying the equilibrium M–N bond length (whilst maintaining constant the stretching force constant and the depth of the Lennard–Jones 12-6 well) until the M–N bond lengths of selected planar metal-

loporphyrins were reproduced. As M(II)OETPP has a saddle shape, each of the alkyl groups can have a pseudo axial or a pseudo equatorial orientation relative to the porphyrin ring; because of the inherent flexibility of the alkyl side chains, and the demonstration that not all conformations of these side chains lead to structures of similar energy, calculations were based on the alkyl side chains placed in the orientations observed in the solid state (i.e. an all pseudo-axial conformation is observed, although this is not the lowest energy conformation predicted by the force field). It was subsequently found [254] that if the force field is augmented to take in electrostatic effects, then the all pseudo-axial conformation is indeed the lowest energy conformation. The agreement between the predicted structures and the solid state structures (where available, viz., Co(II)OETPP and Cu(II)OETPP) was very good. For example, the agreement between the calculated and observed M–N distance, the core size, and the C_α–N–C_α angle was better than 0.01 Å, 0.015 Å and 1.2°, respectively. Importantly, the MM aspects of this study elucidated how a porphyrin can expand to accommodate a larger metal ion. Thus, the C_α–N–C_α angle and C_α–C_m–C_α angles open up and the core size increases to accommodate a larger metal ion. Furthermore, the C_α–C_m and C_β–C_β bond distances can increase by up to 0.01 Å as M(II) changes from Ni(II) to Zn(II).

The highly substituted porphyrin Cu(TC_5T(3,4,5-OMeP)P is completely planar (the Ni(II) analog is only moderately non-planar, as shown by X-ray crystallography [163]); this result, observed crystallographically, was correctly predicted by MM calculations using the Shelnutt force field [163]. By closing the C_β–C_β–CH_2 by some 13° compared to the OEP analogy, the porphyrin is able to move the methylene and aryl substituents apart, obviating the requirement for the extensive ruffling seen in other dodecasubstituted porphyrins.

Resonance Raman observations of structure-sensitive lines and calculations using the Shelnutt force field [255] showed that larger metal ions tend to favor planar porphyrin conformations whereas smaller metal ions induce non-planar distortions, in effect allowing the macrocycle to fold around the metal ion and shorten M–N bond lengths. Increasing the metal radius displaces the non-planar/planar equilibrium of [MOEP]s in solution towards the latter (Ni(II) < Co(II) < Cu(II) < Zn(II)). Even the moderate steric crowding induced by introducing a nitro group in the 5 position of metal-OEPs is sufficient to significantly shift the equilibrium towards the ruffled form. Based on the resonance Raman data, a Boltzmann distribution calculation shows that the energy differences between the planar and non-planar MOEPs and 5-NO_2-MOEPs are very small (ΔE = (non-planar − planar) = −0.29 for M = Ni(II); 0.82 for Co(II); and $\gg$1.37 kcal mol^{-1} for Cu(II)-based on a detection limit of 10% and the failure to observe the non-planar conformation—in [MOEP]; and −0.99 for M = Ni(II); −0.17 for Co(II); and >1.37 kcal mol^{-1} for Cu(II) in [5-NO_2-MOEP]). The degree of out-of-plane distortion increases as the number of *meso* nitro substituents increases [223]; thus, MM calculations show that the projection of the Ni(II)–N bond length onto the mean porphyrin plane, changes from 1.946 Å in NiOEP to 1.957 Å in 5-NO_2–NiOEP, to 1.960 and 1.964 Å in 5,10- and 5,15-$(NO_2)_2$–NiOEP, respectively, to 1.937 Å in 5,10,15-$(NO_2)_3$–NiOEP, and to 1.917 Å in 5,10,15,20-$(NO_2)_4$–NiOEP.

Metal derivatives of TC_6TPP (Ni, Co, Cu) are saddle-shaped and although the porphyrin core expands with increasing metal size, there is little change in the extent of porphyrin distortion [256]; thus, the *trans* N–M–N angles extending across the porphyrin ring, and a measure of the porphyrin saddling, are 165.6, 167.6 and 168.5°, respectively, for MTC_6TPP; M = Ni(II), Co(II), Cu(II). For NiTC_nTPP complexes (n = 5, 6, 7), the porphyrin macrocycle becomes progressively more non-planar as the steric crowding in the periphery increases (*trans* N–M–N = 180.0, 165.6 and 161.6° for n = 5, 6, 7, respectively).

Use was made of a combination of proton NMR spectroscopy and MM calculations to investigate the solution structure of several Co(II) dodecasubstituted porphyrins [224]. The MM calculations showed that the lowest energy conformations of CoOETPP and CoOPTPP, for example, have all ethyl and propyl substituents in quasi-axial orientations (as found in the solid state) such that the alkyl substituents form the walls of a cavity or groove over the porphyrin core. By comparison of the proton paramagnetic shifts measured for these Co(II) porphyrins with the dipolar shifts calculated using geometric factors obtained either from the crystallographic structures (where available) or from the MM energy-minimized structures, these authors showed that the solution structure of these complexes is similar to the crystallographic or MM energy-minimized structures. Porphyrins such as CoOETPP and CoOPTPP that have well-defined cavities in the solid state retain them in solution; consequently, as shown by variable temperature proton NMR spectroscopy, such porphyrins form less stable B complexes with a planar molecule such as 1,3,5-trinitrobenzene than do planar porphyrins such as CoTPP or other less severely distorted porphyrins.

When porphyrins are substituted with flexible groups, as in H_2DAP, the relative orientations of these groups can lead to many conformations very close in energy to each other as demonstrated [248] for ZnDAP. Discovering the global minimum in such cases is not a trivial matter and requires considerable effort and the extensive use of, for example, grid-search and/or dynamics simulations.

Symmetrical porphyrin substitution with sp^3 C groups at the *meso* positions usually results in a *ruf* distortion of the porphyrin. It has been shown by MM calculations using the Shelnutt force field (with some parameter modifications from earlier versions for consistency with the DREIDING II force field and incorporating an exponential-6 van der Waals term for H atoms) and, in some instances, X-ray diffraction crystallography [36], that increasing out-of-plane distortion (as measured by the C_α–N–N–C_α dihedral) occurs as the bulk of the *meso* substituents increases from methyl through to, for example, adamantyl in a series of Ni(II) porphyrins. The MM results were in good agreement with the solid state structures.

Jentzen and Shelnutt [41] have developed a method for classifying and quantifying the in-plane and out-of-plane deformations of the porphyrin macrocycle commonly observed in hemoproteins. Their *normal coordinate structural decomposition* (NSD) method fits any observed distortion to a linear combination of the six lowest-frequency out-of-plane distortion modes of the porphyrin core and, in most cases, this adequately quantifies the porphyrin distortion (Fig. 2). (The distortions can be more accurately simulated by extending the distortion modes to include the second-lowest frequency normal coordinate for all symmetries [257].) The origin of the steric strain responsible for the heme distortions in the tetraheme cytochrome c_3 of sulfate-reducing bacteria was explored using the NSD method after energy-minimizing the heme and amino acid residues immediately attached to the two Cys residues that bridged the iron porphyrin and the protein [258]. They found that the heme distortion is largely controlled by a short peptide segment consisting of the two bridging Cys residues, the amino acids between them, and the proximal His ligand. A similar investigation has been conducted on the structure of nickel cytochrome *c* [259]. For further examples of applications of this NSD method, the interested reader is referred to a recent review [137].

3.1.2. Metal complexes and ligand interactions

There has been considerable interest in the relative orientation of axial ligands in bis-ligated complexes of metalloporphyrins and the effect this has on the structure of porphyrins, since it has been suggested that some bis-histidine multiheme cytochromes such as cytochrome c_3 from *Desulfovibrio vulgaris* are able to fine-tune the redox potential and electronic properties of each heme group by maintaining unique axial ligand orientations, and thus porphyrin conformations [260–263].

The structure of $[Co(TFP)]^+$, $[Co(TClP)]^+$ and $[Co(TMP)]^+$ coordinated in both axial positions by pyridine, 1-methylimidazole, 4-methylpiperidine and isoquinoline was investigated [210] using the program MODELS [211], which allows for relaxation of only a limited number of structural parameters. Both the porphyrin and the axial ligands were treated as planar molecules. By rotating the ligands relative to the porphyrin and performing a series of single point calculations, it was shows that two orientations of the ligand (staggered and eclipsed, Fig. 9) are possible. In agreement with NMR data [210], it was found that for TFP and TPP the preferred orientation of the planar aromatic ligands was the staggered orientation, but increasing the steric bulk of the *meso* substituents in TClP and TMP resulted in the eclipsed conformation being favored.

Munro et al. [162] demonstrated, using a modified version of MM2(87) and the Munro force field (see above) that *trans* axial imidazole ligands whose planes are approximately perpendicular to each other and bisect the *cis* N–Fe–N angles of the metalloporphyrin core, induce a *ruf* conformation. The extent of the ruffling increases with the shortening of the Fe–N_{ax} bond length by the van der Waals contacts between the porphyrin core and the axial ligand.

Two crystalline forms of $[Fe(TMP)(5\text{-}MeHIm)_2]ClO_4$ have been observed [264]. In the first form, the two imidazole ligands are virtually parallel to each other and lie close to an N_{porph}–Fe–N_{porph} vector; the core is slightly S_4 ruffled. In the second form, the imidazole ligands are virtually perpendicular to each other and each lies close to a C_{meso}–Fe–C_{meso} vector. As a consequence, the porphyrin is markedly S_4 ruffled. MM calculations show that steric interaction between the axial ligands and the *meso* substituents destabilize the mutually parallel structure by 2.6 kcal mol^{-1}, yet this form is always that observed by ESR spectroscopy in frozen solution samples. There therefore appears to be competition between this steric factor and an electronic stabilization (2.8–3.7 kcal mol^{-1}) of the rhombically (Jahn–Teller) distorted electronic ground state of the mutually parallel structure.

Marques et al. [265] adapted parameters from the Munro force field to the version of MM2 used in the

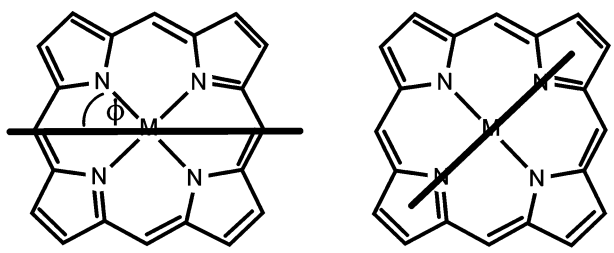

Fig. 9. The staggered and eclipsed conformations of a planar aromatic ligand relative to the porphyrin core. The dihedral angle ϕ is used to quantify the orientation of the ligand.

HYPERCHEM suite of programs (Hypercube, Inc., Gainesville, FL) and known as MM+ to examine the structure of complexes formed between the heme octapeptide *N*-acetylmicroperoxidase-8 and quinine, 9-epiquine and chloroquine, as it is widely believed that ferriprotoporphyrin IX is the target for antimalarials [266]. It was shown that coordination of the 9-alkoxide group to Fe(III) is possible for both quinine and 9-epiquine, with the quinoline ring system virtually parallel to the porphyrin plane. The energy-minimized structure for the interaction of a chloroquine molecule with the heme peptide has a B complex formed between the quinoline and the porphyrin rings.

New parameters [267] have been added to the Munro force field for the modeling of low spin Fe(II) porphyrins carrying two axial primary amine ligands. MM calculations show that the most stable conformations have the α-carbons of the axial ligands directly over, and the α-CH_2 and NH_2 protons staggered about, the Fe–N_{porph} bonds. There is a low barrier to rotation of the axial ligand (<0.5 kcal mol^{-1}) and deviations of the solid state structures of [Fe(TPP)($BzNH_2$)$_2$] and [Fe(TPP)(1-$BuNH_2$)$_2$] from the MM-calculated global minima are shown to be a consequence of packing in the crystal.

The Munro force field [162,164,165] was used by Momot and Walker [268] to investigate the rate of axial ligand rotation in [Fe(TMP)(1,2-Me_2Im)$_2$]$^+$ and [Fe(TPP)(1-MeIm)$_2$]$^+$. A variety of NMR experiments showed that the rotational energy barrier for the axial ligands in [Fe(TMP)(2-MeHIm)$_2$]$^+$ is 12.0–14.1 kcal mol^{-1} and $\Delta S^{\ddagger} = 0.7$–$9.8$ cal K^{-1} mol^{-1}. Using both a dihedral drive method and Monte Carlo single minimum analysis with subsequent geometry optimization, it was shown that the preferred mode of rotation for the imidazole ligands in [Fe(TMP)(1,2-Me_2Im)$_2$]$^+$ is synchronous rotation of mutually perpendicular ligands, and that the enthalpy barrier to such rotation is about 11.5 kcal mol^{-1}, in very reasonable agreement with the experimental result for [Fe(TMP)(2-MeHIm)$_2$]$^+$. For the unhindered ligands in [Fe(TPP)(1-MeIm)$_2$]$^+$, enthalpy barriers to synchronous and asynchronous rotation were found to be 0.8 and 1.3 kcal mol^{-1}, respectively. The rate of rotation is thus about 10^{12} s^{-1}, which is very fast on the NMR time scale, again consistent with the NMR experimental observations. The authors concluded that MM methods are potentially useful and adequate for studying the rotation of axial ligands in six-coordinate porphyrin complexes.

Highly substituted porphyrins such as [Co(T^{t}BuP)]$^+$ and [Co(OETPP)]$^+$ are very non-planar (see below) and they fold such that the peripheral substituents form cavities on the porphyrin faces. Planar axial ligands such as pyridines and imidazoles are expected to occupy these cavities. Thus MM calculations on complexes of the type [Co(OETPP)(L_2)]$^+$, L = an imidazole or a pyridine, were predicted [269,270], using the Shelnutt force field, to have the ligand planes mutually perpendicular and parallel to the N_{porph}–Co–N_{porph} vector, whereas in [Co(T^{t}BuP)(L_2)]$^+$, the ligands, also mutually perpendicular to each other, lie along the C_{meso}–Co–C_{meso} vectors. The MM predictions were confirmed by NMR observations [269] and the initial predictions were borne out by X-ray structure determinations [271].

The Shelnutt force field has been used as part of an investigation into the effect of axial coordination by pyrrolidine and piperidine in NiTPP complexes [272]. The ligands are relatively free to rotate so the different conformations coexist in solution, as confirmed by their resonance Raman spectra. Five coordinate complexes are slightly domed. If the plane of the axial ligand bisects Ni–N_{porph} bonds, the porphyrin is ruffled; when it is aligned with the Ni–N_{porph} bond, a saddling deformation occurs. Adding a second ligand causes the doming to disappear, and the distortion of the porphyrin depends on whether the ligand planes are parallel or perpendicular to each other. In all cases, differences in energy between the identified conformations are small and the authors suggest that the orientation of axial ligands in, for example, the *c*-type cytochromes, play only a small role in eliciting the non-planarity of the porphyrin observed in many of these hemoproteins.

Whilst MM methods are clearly useful for investigating the influence of axial ligands on the conformation of the porphyrin core, perhaps a word of caution is appropriate. In an attempt to investigate a proposed mechanism for P_{450}-catalyzed hydroxylation of alkanes, Yoshizawa and co-workers used the UFF force field to predict structures of intermediates which involve binding of both the oxygen of the oxyferryl group and the alkane reactant to Fe(IV) on the distal face of the porphyrin [225]. This required the loss of the proximal thiolate ligand and the distortion of the porphyrin into (at least in the view of the present authors) an unlikely and unprecedented highly strained conformation in order to accommodate near octahedral geometry at the metal. We suggest that the UFF force field is not, and has never been shown to be, sufficiently well-parameterized to reliably reproduce porphyrin structures.

3.1.3. Metal-free porphyrins and related compounds

Bruice and co-workers [194] explored the relationship between the ^{1}H-NMR and electronic spectral properties of cofacial metal-free porphyrin dimers and the distance between the porphyrin planes, using MM to determine the inter-porphyrin separation of a series of symmetrical and unsymmetrical quadruply three- (*m*-$C_6H_4CH_2$-N(R)CH_2–*m*-C_6H_4) and five-atom (*m*-C_6H_4–CH_2O–C-

(O)–OCH_2–*m*-C_6H_4) aza-bridged TPP derivatives. The structures determined from molecular dynamics simulations with the CHARMm force field were shown to be very similar to those predicted by semi-empirical methods and, in one particular case where R = 3-*N*-methylpyridyl, in agreement with the solution structure determined from the ROESY spectrum [195]. The minimum energy structures found entail the folding of the linker arms such that the two porphyrins are in a screwed down conformation. The size and shape of the cavity between the two porphyrin rings depends on the nature of R in the linker. Where R is large (such as *P*-toluenesulfonamide or *m*-pyridinesulfonamide), the interplanar distance of the porphyrin cores are shorter than in the case of small groups such as cyanamide. The hybridization of the bridging N is also a critical factor; the greater the sp^3 character, the more flexible the geometry, and the shorter the interplanar distance. Molecular dynamics simulations show, as expected, that the flexibility of the structure depends on the number of linkages between the two porphyrins [195]. As part of this study, the authors explored the interaction energy between two porphyrins as a function of the interplanar distance and the dihedral angle $\phi = N_1$–Ct_1–Ct_2–N_2. The resulting three-dimensional energy surface had an energy minimum at $\phi = 26°$ and an inter-planar distance of 4.6 Å; if the *meso* phenyl substituents were excluded, then a fully eclipsed conformation ($\phi = 0°$) is marginally favored, with an interplanar distance of 3.5 Å, close to twice the van der Waals radius of carbon, and in agreement with crystallographic evidence.

The ground state structure of terakis(*N*-methylpyridyl)porphyrins has been explored using the CHARMm force field [196]. The fluorescence lifetimes of H_2T(*n*-*N*-MPy)P, $n = 2$, 3, 4, in solution and when adsorbed onto a solid surface, can be explained by the barrier to rotation of the *meso* pyridinium groups relative to the porphyrin core, which MM calculations show is greatest when $n = 2$.

Connolly and co-workers [197] used MM calculations to determine the ground state structure of a series of *meso*-substituted tetra-alkyl and tetra-aryl free base porphyrins, and were able to rationalize the observed trends in the red shifts of the absorption and fluorescence bands, as well as the quantum yields, on the extent of mixing between the substituent π electron system with that of the porphyrin (as deduced from the dihedral angle between these entities) and on the degree of non-planarity of the porphyrin ring.

A series of isomeric (*ortho*-, *meta*- and *para*-) nitrobenzyl mono- and diesters of *meso*-porphyrin have been synthesized [198] and their structures investigated by MM and semiempirical MO methods (using the AM1 model). The nitrobenzyl groups are linked through one or both propionate side chains of the porphyrin. In the energy-minimized structure, discovered by MM and molecular dynamics methods, each benzyl group lies approximately parallel to the porphyrin ring, but significant structural differences exist between the *ortho*-, *meta*- and *para*-complexes. The authors consider the implication of these structural differences for the photoinduced electron transfer efficiency of these complexes.

Battersby and co-workers [200] used the MM2 force field to estimate the potential energy barrier to the interconversion of two putative atropisomers of a minor product obtained during the synthesis of a spirolactone related to the spiro-intermediate along the biosynthetic pathway to uroporphyrinogen III synthesis. Since the calculated energy barriers were modest (< 8 kcal mol^{-1}), the two isomers should interconvert rapidly at room temperature. This led to a re-investigation of the nature of this minor product and to its eventual elucidation as a dimeric species.

Casiraghi et al. [204] investigated the structure of a 5,15-bis-phenyl, 10,20-bis-glycosylated porphyrin (5,15-[bis(4-flurophenyl)]-10,20-[bis(1,2,4-tri-*O*-benzyl-D-*arabino*-tetritol-1-yl]porphyrin) using the CVFF force field. In agreement with 2D NMR data, the metal-free porphyrin was shown to exist in a *sad* conformation.

The structure of some metal-free porphyrins distorted by strapping neighboring *meso* *o*-phenoxy groups either with *cis* or *trans* linkages has been investigated using the AMBER force field [205]. When the two short linkages are *cis* to each other, the porphyrin adopts a *sad* conformation; *trans* linkages lead to the *ruf* conformation. The assumption was made that introduction of Fe(III) did not lead to a substantial change in conformation, and the spectral properties (electronic, IR, NMR) of these metalloporphyrins and their π-cation radicals were compared to the properties of $[FeTPP]^+$ to show the effect of porphyrin distortion from planarity. In a related study [206], the structure of similar metal-free porphyrins, and porphyrins where the distortion from planarity was induced by strapping across opposite *meso* phenyl substituents, was explored. The influence of non-planarity on the triplet state characteristics of these free base porphyrins and their Zn(II) analogs (where it was again assumed that introduction of the metal ion does not significantly perturb the porphyrin structure) was investigated by ESR spectroscopy. The population and decay of the triplet sublevels is dependent on the non-planarity of the porphyrin core. Moreover, distortion in these basket handle porphyrins results in a red shift of the fluorescence emission bands, low quantum yields, high intersystem crossing rates, and markedly shorter first excited singlet state lifetimes [207]. The distorting effect of the basket handles is augmented by substitution of H by Br at the β-pyrrole positions.

Bonar-Law and Sanders [202] used the MM2 and AMBER force fields to explore the structures of novel porphyrins capped with a cyclic dilactone of cholic acid (a 7,24-cyclo[2]cholate). The structures were then used to help with calculations of porphyrin-induced NMR shifts using the approach of Abraham [273].

Cheng et al. [166] modified the parameters of the Munro force field for the modeling of porphyrin diacids, making some adjustments to a number of torsional parameters. The parametrization was based on the crystal structures of three diacids, $[H_4OEP]^{2+}$, $[H_4TPP]^{2+}$ and $[H_4TMP]^{2+}$. The calculations indicated that distortion from planarity decreases as the steric bulk of the peripheral substituents increases: $[H_4TPyP]^{2+} \approx [H_4TPP]^{2+} > [H_4T\text{-}2,6\text{-}(OH)_2PP]^{2+} \approx [H_4T\text{-}2,6\text{-}F_2PP]^{2+} > [H_4T\text{-}2,6\text{-}Cl_2PP]^{2+} \approx [H_4TMP]^{2+}$. Depending on the relative orientations of the *meso* tetraaryl substituents, pairs of inversion related minima with D_{2d}-saddled and C_{2h}-stepped core conformations were found on grid-searching the structures of $[H_4porphine]^{2+}$, $[H_4OEP]^{2+}$, $[H_4TPP]^{2+}$ and $[H_4T\text{–}2,6\text{-}Cl_2PP]^{2+}$. The strain energy barrier to inversion of the lowest energy D_{2d}-saddled conformation increases from 0.45 kcal mol^{-1} in $[H_4porphine]^{2+}$ to 1.9 kcal mol^{-1} in $[H_4T\text{–}2,6\text{-}Cl_2PP]^{2+}$. The stability of the D_{2d}-saddled isomer relative to the C_{2h}-stepped isomer increased from -0.8 kcal mol^{-1} for $[H_4porphine]^{2+}$ to -1.8 kcal mol^{-1} in $[H_4T\text{–}2,6\text{-}Cl_2PP]^{2+}$.

The structure of a heavily substituted rosarin (an expanded porphyrin), 4,9,13,18,22,17-hexaethyl-5,8,14, 17,23,26-hexamethyl-2,11,20-triphenylrosarin, was investigated using the MM+ force field prior to semi-empirical MO calculations which, within the accuracy of the INDO/S method, correctly predicted the absorption spectrum of this compound [199].

Panday and co-workers [209] have recently synthesized a spirochlorin–chlorin dimer with a fixed distance between the two chlorins as a model for the special pair of the photosynthetic reaction center. The structure of the dimer was explored using the SYBYL force field and it was shown that the single pyrrole overlap of the two chlorins closely matches that found crystallographically in the reaction center.

3.1.4. The best-fit metal ion in a porphyrin

Scott and co-workers [216] used the MM2 force field and Hancock's approach [274] to evaluate the effect of reduction of Ni(II)-containing porphyrin-type macrocycles. They found that reduction at β-pyrrole positions causes an increase in the size of the macrocycle core but no change in its flexibility (ability to undergo S_4 ruffling), but reduction at methine positions results in a decrease in core size, and an increase in flexibility. Flexibility was assessed by the steepness of the strain energy versus Ni–N bond length response curve. The reduction at two neighboring methine carbons in F_{430}, the Ni(II)-containing cofactor of the *S*-methyl coenzyme M reductase enzyme system of methanogenic bacteria, results in a very flexible macrocycle, indeed the most flexible of those investigated (porphyrin, chlorin, isobacteriochlorin, pyrrocorphin, hexahydroporphyrin). This provides the F_{430} system with the flexibility needed to accommodate both high spin 6-coordinate Ni(II) and low spin 4-coordinate square-planar Ni(II), and rationalizes the relatively high affinity of the system for axial ligands. Moreover, since Ni(I) is larger than Ni(II), it is speculated that the flexibility of the macrocycle might aid in a physiological redox role for F_{430}. Interestingly, F_{430} does not have a larger core than more oxidized (hydro)porphyrins; hence core expansion is not the reason for F_{430}'s increased affinity for axial ligands.

Crystallographic data for a variety of metalloporphyrins indicate that a planar porphyrin core will occur with M–N bond lengths of between 1.96 and 2.08 Å [162]. The best-fit size of a metal ion in a planar porphyrin core was determined by varying the equilibrium M–N bond length, l_0, between these limits, whilst maintaining a constant value for the M–N stretching force constant, and plotting the total strain energy as a function of l_0. This gave a parabolic response curve with a minimum at 2.035 Å, in agreement with a suggestion [275] that the ideal M–N bond length for coordination is the porphyrin ring is between 2.01 and 2.04 Å.

3.1.5. The change in spin state of Fe(II)

An important aspect of the cooperativity model of hemoglobin [276] entails Fe(II) rising out of the mean porphyrin plane on deoxygenation. Is this a consequence of high spin Fe(II) attempting to escape the constraints of the macrocycle? Munro et al. [162] explored the importance of steric factors in the absence of axial ligands by modeling [Fe(porphine)]. Starting with a planar structure and parameters appropriate for low spin Fe(II), energy minimization led to a planar structure with a porphyrin cavity (N_1–N_3) of 3.985 Å. Changing parameters to those appropriate for low spin Fe(II) lead to a minimized structure with an expanded cavity (4.156 Å) with the metal virtually in the plane of the four pyrrole Ns. When the starting structure had the metal ion slightly above the mean porphyrin plane, the energy-minimized structure was C_{2v} domed with a fold along the N_2–Fe–N_4 vector; pyrroles 2 and 4 were virtually in the mean porphyrin plane, whilst pyrroles 1 and 3 were below the plane. The metal–Ct distance was 0.32 Å, and the porphyrin cavity was 4.103 Å. The domed structure was found to be only 1.3 kcal mol^{-1} more stable than the planar structure. Thus, at the expense of a very modest energy penalty, the porphyrin core is quite capable of expanding to accommodate an increase in ionic radius as Fe(II) changes from low spin

to high spin on oxygenation. Evidently, the drive to a domed structure is not steric, but electronic, as this will maximize orbital overlap between the metal and the N donor of the proximal His ligand.

3.1.6. N-substituted porphyrins

The flexibility of the Shelnutt force field was demonstrated with an investigation of the structure of four of the eight possible regional isomers of protoporphyrin IX dimethyl ester substituted with phenyl at each of the four *N*-pyrrole positions [277]. Interest in these compounds stems from the fact that *N*-substitution of the ferric porphyrin in cytochrome P_{450} on reaction with various xenobiotics causes enzyme inactivation, and *N*-substituted porphyrins inhibit the enzyme ferrochelatase. It was found that the only parameter that needed to be adjusted to accurately model Zn(II)(Cl)–*N*-phenyltetraphenylporphyrin was the Zn–N(substituted) equilibrium bond length, which had to be increased by nearly 1 Å. The structures of the four *N*-substituted protoporphyrin IX derivatives, in which the phenyl is on the distal side of the porphyrin, revealed that an asymmetric distortion results from addition of the phenyl substituent. In particular, the tilting of the substituted pyrrole ring leads to a decrease in the extent of the porphyrin B conjugation; this could be correlated with shifts in the structure-sensitive lines of the resonance Raman spectrum.

3.1.7. Interaction with substrates

Two complexes of deuterohemin, deuterohemin–2(18)-glycyl-L-histidine methyl ester (DH–GH) and deuterohemin–2,18-bis(glycyl-L-histidine) dimethyl ester (DH–$(GH)_2$) were synthesized by condensation of glycyl-L-histidine methyl ester on the propanoic acid side chains of deuterohemin [278]. The structures of the complexes were investigated using the CVFF force field [203], extended [215] for the study of iron porphyrins. DH–Gh is a catalyst for the oxidation of phenols by H_2O_2. The reactions are stereoselective, suggesting an interaction of the substrate with chiral His on the proximal face of the porphyrin. Molecular dynamics and SA calculations were used to test this possibility (see below) and minimum energy structures were found where the substrate does indeed interact with the chiral center of the porphyrin, rationalizing the experimental observations.

3.1.8. Dimeric porphyrins

The dimeric porphyrin, $[Fe(OEP)]_2O$, crystallizes in two polymorphs [279]; in both, surprisingly, the porphyrin rings are in a near-eclipsed conformation (the N–Fe–Fe′–N′ dihedrals are 17.0 and 16.8°, respectively, in the crystalline forms). MM calculations using the Shelnutt force field accurately reproduced the structural features, including the average displacement of the ferric ions from their respective mean porphyrin planes, the average porphyrin–porphyrin separation and the interplanar angles between the porphyrins. Importantly, the MM calculations reproduce the eclipsed conformation. By changing the orientation of the peripheral ethyl groups, the N–Fe–Fe′–N′ dihedral could be increased to 31.6°, thus showing that the eclipsed conformation is largely a response to the steric dictates of the porphyrin substituents.

3.1.9. Crystal structure effects

The effect of crystal packing forces and π–π interactions on the structure of CuOEP and NiOEP has been investigated [222]. Only very minor effects were found. The differences between the crystallographically-observed and calculated structures (where calculations were performed on an isolated molecule and therefore necessarily exclude crystal packing and π–π effects) were insignificant, with the exception of NiOEP in which the ethyl substituents were placed in the orientation observed in the tetragonal crystalline form of NiOEP. Whereas calculations predicted a perfectly planar porphyrin ($N_\alpha C–CN_\alpha = 0.0°$), the crystal structure is non-planar distorted (31.8°). The *ruff* distortion mode is considered to be a 'soft' mode, and it was suggested that packing forces were sufficient to allow crystallization in an energetically unfavorable conformation. A further effect of the solid state was a reversal in the trend of M–N bond lengths with respect to the stacking axis in the crystal. For example, in the triclinic B form of NiOEP, the Ni–N bond lengths are 1.946 and 1.958 Å, with the shorter and longer lengths, respectively, parallel and perpendicular to the stacking axis. The calculation predicts lengths of 1.951 and 1.954 Å where the marginally longer distance corresponds to the stacking axis.

3.1.10. 'Designer' porphyrins

In principle, once a reliable force field has been developed, it can be used as a useful tool in directing synthetic endeavors towards compounds with desired properties. An example of this is the design and synthesis by Shelnutt and co-workers [280] of a Ni(II)–lipoporphyrin, NiLipoP (octakis((methoxy–carbonyl)-methyl)-*meso*-tetrakis(((eicosanyloxy)carbonyl)phenyl)-porphyrin) with a ruffled porphyrin head (to minimize π–π aggregation in aqueous solution) and 20-carbon long nonpolar tails to anchor the species into stearic acid films. The head group can be modified for binding to target molecules or to have specific photochemical or photoelectrochemical activity. Molecular dynamics simulations, including solvent water molecules, were used to rationalize the experimental observations on the NiLipoP-stearic acid films; the model has a non-planar porphyrin protruding from the film, correctly orientated for target molecule binding, and with no π interaction with neighboring porphyrins.

3.2. Structure predictions: cobalt corrinoids

The development of a reliable force field for the modeling of the cobalt corrinoids by Marques and co-workers [228] led to the exploration of a variety of questions concerning the structure of these complexes. Some of the highlights of this work are reviewed briefly below, principally to indicate to the reader the scope to which MM methods have been put; for a more extensive review see Ref. [281].

3.2.1. Alkylcobalamins

The standard force field parameter set used for modeling the cobalt corrinoids was extended with the development of parameters for modeling the Co–C bond length and the Co–C–C bond angle [282]. The accessible conformations of methyl-, adenosyl-, benzyl- and neopentylcobalamin were explored and a set of probable conformations for each complex was determined. A Boltzmann distribution was applied to these conformations to obtain a population-weighted value of the Co–C bond length and Co–C–X bond angle (X = C, H). It was found that the steric demands of the four alkyl ligands increased in the order Me < Bz ≈ Ado < Np, as could be gauged from the Co–C bond length and Co–C–X bond angle. An inverse relationship between the Co–C bond dissociation energy and the steric strain on the alkyl moiety was demonstrated; thus, when an alkyl ligand is bound to Co(III) in an alkylcobalamin, the steric strain on the ligand leads to an elongation of the Co–C bond length and the distortion of the Co–C–X bond angle. Calculations show that this strain is relieved, or partially relieved, as the transition state is approached and this therefore suggests that labilization of the Co–C bond, a key feature of the AdoCbl-dependent enzymatic reactions, could be achieved by the distortion of the Co–C–C bond angle [283–286] or the stretching of the Co–C bond by the protein, possibly by an upward flexing of the corrin ring [287–290].

In a recent extension of this work [291], the feasibility of such a mechanochemical triggering mechanism was explored. This mechanism envisions enzymatic compression of the long (2.23 Å) axial Co–N bond of AdoCbl and a consequent increase in the steric interactions of the bulky bzm ligand with the underside of the corrin; this in turn would increase the latter's upward fold, in turn causing elongation of the Co–C bond and/or opening of the Co–C–C angle. Both MM and semi-empirical MO calculations were used. It was found that both in CH_3Cbl and AdoCbl, compression of the axial Co–N bond does indeed cause an increase in the upward fold of the corrin ring; moreover, the extent of the induced fold is smaller if bzm is replaced by imidazole. In AdoCbl, both the Co–C bond length and the Co–C–C bond angle respond by increasing, but the effect is estimated to contribute at most some 3 kcal mol^{-1} towards enzymatic catalysis of Co–C bond homolysis, far short of the ca. 14 kcal mol^{-1} required. Thus, what might be termed ground state mechanochemical-triggering, seems to be unlikely as a complete explanation for Co–C bond homolysis (Fig. 10A). However, there is a second possibility; that of transition state mechanochemical-triggering (Fig. 10B) [291]. In

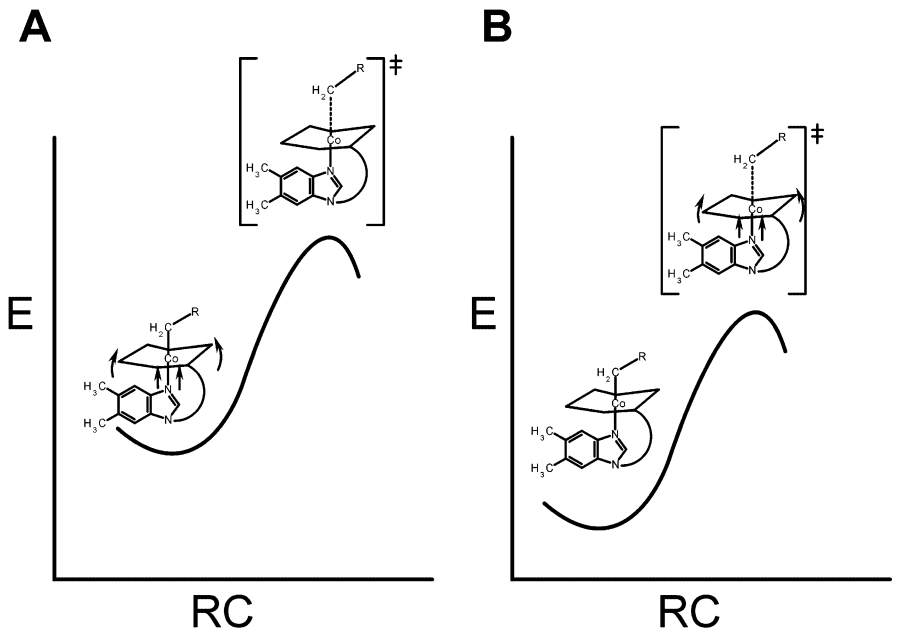

Fig. 10. Mechanochemical-triggering can be effected by (A) destabilization of the ground state of a cobalamin or (B) stabilization of the transition state.

this scenario, the transition state is stabilized *electronically* by increased orbital overlap between the axial ligand and the metal as the enzyme sterically compresses the axial Co–N bond. The Co–C bond was stretched to simulate the approach to the transition state; this was found to result in an upward folding of the corrin ring, a slight decrease in the axial Co–N bond length, a slight displacement of the metal atom from the plane of the equatorial nitrogens towards the lower axial ligand, and a decrease in strain energy amounting to about 8 kcal mol^{-1} for both AdoCbl and Ado(Im)Cbl (in which the proximal bzm ligand was replaced by imidazole, to simulate the displacement of bzm by His in the Class I enzymes—see above). In such modeled transition states, compression of the axial Co–N bond to just below 2.0 Å (the distance found to provide maximal stabilization of the transition state by increased orbital overlap—see below) required about 4 kcal mol^{-1} for AdoCbl, and about 2.5 kcal mol^{-1} for Ado(Im)Cbl. ZINDO/1 calculations [292,293] showed that maximal electronic stabilization of the transition state by about 10 kcal mol^{-1} occurred at an axial Co–N bond distance of 1.96 Å for both AdoCbl and Ado(Im)Cbl. The net result is that this type of transition state mechanochemical triggering can provide 14 kcal mol^{-1} of transition state stabilization for AdoCbl, and about 15.5 kcal mol^{-1} for the Ado(Im)Cbl; enough to completely explain the observed enzymatic catalysis.

Finke and co-workers [170] have also used MM methods (with the UFF) to investigate the feasibility of an axial-base-driven, sterically-induced corrin fold to account for Co–C bond homolysis. They found that decreasing the Co–N axial bond of AdoCbl from 4.5 to 1.44 Å does indeed cause elongation of the Co–C bond and an opening of the Co–C–C angle, but they concluded this could account for, at most, about 1/3 the effect needed to explain the observed acceleration of Co–C bond homolysis in the enzyme. They suggest that a combination of effects may be required to explain the catalysis, including an enzyme-induced upward folding of the corrin ring, and a coupling of Co–C bond cleavage to substrate or cystein S–H bond cleavage and Ado–H bond formation steps.

3.2.2. The corrin side chains and homolysis of the Co–C bond

The Co–C bond in the base-on alkylcobalamins is 2–3 orders of magnitude more labile towards thermolysis than in the base-off alkylcobalamins [294–296]. Since the difference in reactivity was found to be largely due to differences in the entropy of activation, this led to the hypothesis that the thermal motions of the upwardly-projecting acetamide side chains play an important role in the entropic activation of alkylcobalamin homolysis. In this hypothesis, these motions are restricted by the alkyl ligand and the restrictions are relieved—or partially relieved—on approaching the transition state as Co(II) and the alkyl radical begin to separate. In those species in which the bzm is either missing (the cobinamides) or not coordinated (the base-off cobalamins), the flattening of the flexible corrin ring would reduce the restriction on the acetamide side chain mobility, increase the ground state entropy and, compared to base-on species, diminish the relative entropy increase as the transition state is approached.

In order to test this hypothesis, a series of neopentylcobalamins with different groups in the *c* side amide were synthesized and the kinetics of the thermolysis studied [297]. Whilst $\Delta H^{\ddagger}$ remained largely constant for the process, $\Delta S^{\ddagger}$ increased with the bulk of the *c* side chain substituent. MM calculations showed that the Co–C bond length, and the Co–C–C and Co–C–H bond angles, were not altered significantly either by rotation of the *c* side chain through 360° about the C7–C37 bond or by increasing the bulk of the *c* side chain substituent. This is in agreement with the observation that $\Delta H^{\ddagger}$ remains essentially constant for the series of compounds. The total strain for rotation of the *c* side chain about the C7–C37 bond increases monotonically with the steric bulk of the *c* side chain substituent, and decreases with Co–C distance as the metal and alkyl radical begin to separate on approaching the transition state. Thus, as the bulk of the side chain increases, fewer and fewer conformations are available to it, and the ground state entropy decreases. Based on these results, it was deduced that up to 40% of the decrease in ΔG for thermolysis of AdoCbl brought about by enzyme catalysis could be accounted for by enzyme-induced restriction of the motion of the acetamide side chains in the ground state, and the partial relief of these restrictions in the transition state [297,298].

It is interesting to note (Fig. 11) that in the reported crystal structure of methylmalonyl coenzyme A mutase [94] the acetamide side chains are located in relatively open pockets of the protein, and are not hydrogen bonded to protein residues (only the *e* propionamide side chain is hydrogen bonded, to the amino proton of Asp 611). Relatively free motion appears possible, which might be curtailed by a conformational change of the protein.

3.2.3. Compounds that do not crystallize: Ado-13-epiCbl

The use of MM with a reliable force field may be the only viable way of exploring the structure of compounds that stubbornly refuse to crystallize. Thus, the structure of Ado-13-epiCbl, a coenzymatically-active structural analog of AdoCbl in which the *e* side chain has been epimerized from the α face of the corrin ring, fails to crystallize; its structure was examined by MM

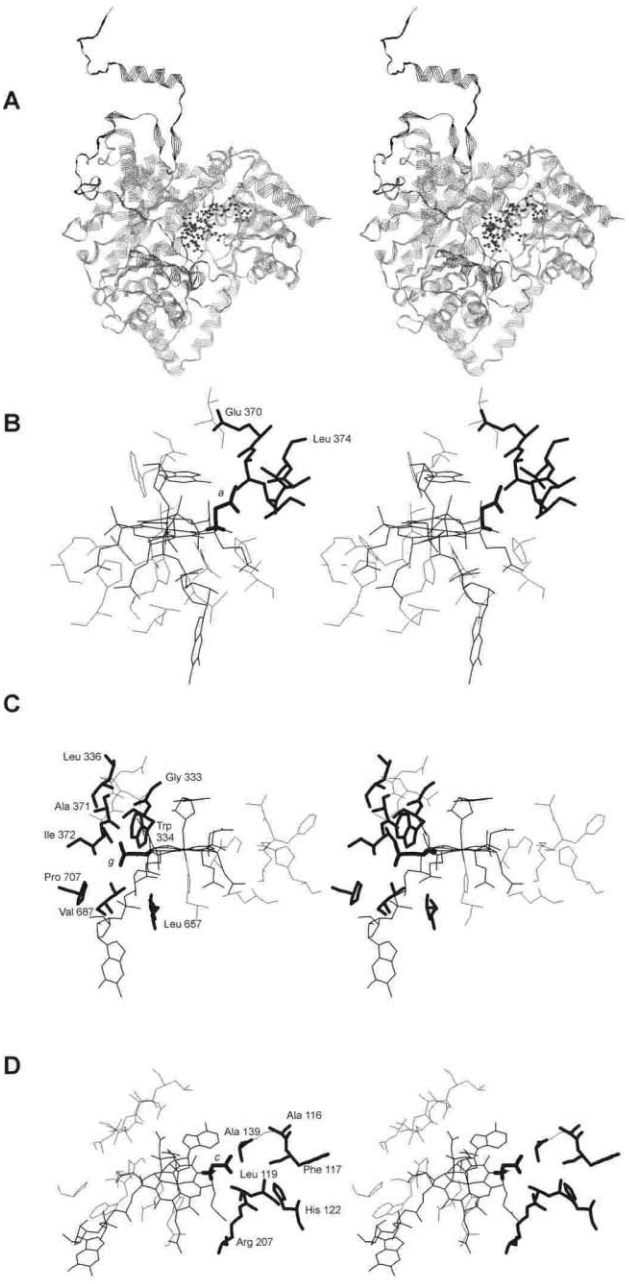

Fig. 11. The acetamide side chains of AdoCbl in methylmalonyl coenzyme A mutase. A: Cartoon diagram of the α chain of the protein showing the location of base-off AdoCbl. His 610 is the α ligand of Co(III) and the nucleotide loop is buried in a cleft. In the stereoviews B–D the amino acid residues within 7 Å of the highlighted side chain are shown in bold lines. B: The *a* side chain is located in a pocket bound by the adenine moiety of the coordinated Ado ligand and four amino acid residues (Glu 370 to Leu 374) of a random loop of the protein. C: The *f* side chain and a number of residues (Leu 336, Gly 333, Trp 334, Ala 371, Ile 372, Leu 657, Val 687 and Pro 707) form a pocket in which the *g* side chain is located. D: The *c* side chain is bound by the adenine moiety, and by Arg 207, His 122, Phe 117, Ala 116, Ala 139 and Leu 119.

methods [299]. In this species, the western conformation was found to be the global minimum (Fig. 12), but three other conformations (a northern, a northeastern and an eastern conformation) are close in energy. The southern conformation is destabilized by some 6 kcal mol^{-1} relative to the western conformation, with the *e* side chain (which occupies a pseudo equatorial position) and the adenine moiety moving away from each other, and causing an opening of the Co–C–C bond angle. There are many more nOe NMR crosspeaks between Ado and non-Ado protons in the 13-epimer than in AdoCbl itself, which attests to the considerable conformational flexibility of this compound in solution. The crosspeaks and the interproton distances measured from the MM structures suggest that all four conformations are populated in solution. Since 13-*epi*-AdoCbl is coenzymatically-active and the southern conformation is apparently inaccessible, this raises questions about the active conformation of AdoCbl when bound to the protein in the AdoCbl-dependent enzymes. In this regard, it may be noted that in methylmalonyl coenzyme A mutase [94] the Ado ligand is in a northern conformation.

3.2.4. MM and directed synthesis: (α-ribo)AdoCbl

MM methods can be used to explore the probable stability of novel compounds before embarking on a time-consuming synthetic endeavor. Thus, the probable structure of a new analog of coenzyme B_{12} in which the configuration of the *N*-glycosidic bond in the Ado ligand is inverted, (α-ribo)AdoCbl, was predicted computationally [300]; only thereafter was a synthesis attempted. This was successfully completed, the compound crystallized, and the structure determined by diffraction methods. There was good agreement between the crystal structure and the MM-predicted structure, except for the disorder observed in the adenine moiety in the solid state (Fig. 13).

3.3. MD simulations: hemes and hemoproteins

Molecular dynamics methods [189,301,302] attempt to reproduce the dynamic behavior of molecular systems by computing a dynamics trajectory. The future positions and velocities of atoms are predicted based on their current positions and velocities by solving the classical equations of motion. A variety of algorithms, such as the leap-frog algorithm [190,303] is used to solve the equations. By varying the temperature at which the simulation is performed, the extent of the motion can be controlled. It is quite common to perform simulations by first heating the molecule from a low temperature to an artificially high temperature (600 to 1000 K is usual), and then performing the run phase of the simulation at this temperature. The high temperatures facilitate the surmounting of potential energy

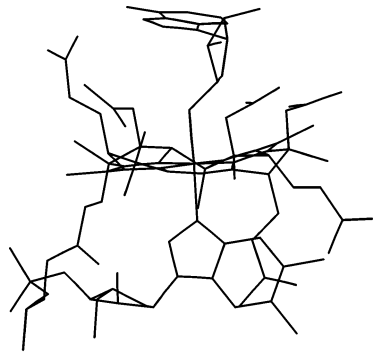

Fig. 12. The western conformation of Ado-13-epiCbl predicted by MM methods. The view is from C10 towards the C1–C19 bridge. The availability of a reliable force field makes MM methods viable means of exploring the structure of molecules that fail to crystallize.

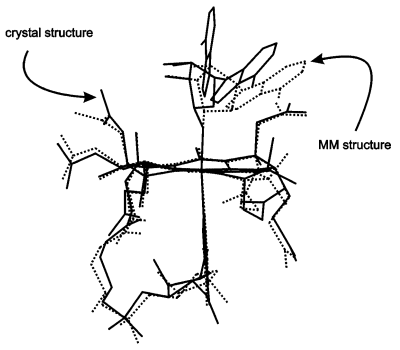

Fig. 13. A comparison of the crystal structure of (α-ribo)AdoCbl and the MM-predicted structure.

barriers. In a quenched dynamics simulation, samples of the conformation are taken at random or fixed intervals, fully energy-minimized, compared and sorted, and new conformations are stored. Alternatively, in a SA procedure [191], the system is slowly cooled after the run phase, and then fully energy-minimized. In order to limit the extent of conformational space that has to be searched, restraints may be applied to an MD simulation, in effect limiting the search to those regions of conformation space that satisfy some experimental observations. An example of this is the adding of dummy bonds or restraints (usually using simple parabolic functions) between protons to limit the proton–proton distance to particular values based on nOe observations from 2D NMR experiments [304]. The nOe crosspeaks are classified as strong, medium, weak or very weak depending on the mixing time at which they first appear in the ROESY spectrum and an appropriate force constant used for each class of nOe. H–H distance criteria commensurate with the observed strength of the nOe have been defined [305].

3.3.1. Molecular dynamics simulations of hemes and hemoproteins

Molecular dynamics simulations of biological macromolecules provide insight into the internal motions of these molecules, including domain–domain and residue–residue interactions, and the structure of internal water molecules. They also allow the investigator to explore the effect of such factors as point mutations, and binding of substrates and inhibitors on the dynamics of the macromolecule. As such, MD simulations may allow, in favorable circumstances, for a better understanding of biological function. It must be appreciated, however, that with present computer resources simulations are only possible up to an order of a nanosecond and processes that take longer than this either cannot be studied or can only be studied under non-equilibrium conditions. Various procedures may be employed to cut down the amount of computer time required; these include the use of united atom force fields, and cut-offs such that pair-wise interactions at greater than some given distance (10 Å is often used) are set to zero. This does not significantly alter the order of magnitude of dynamics processes currently amenable to investigation.

Commonly-used force fields usually do not have parameters for handling metal ions. Hence, before meaningful results can be obtained, an adequate parameterization is mandatory, as described above in the modeling of metalloporphyrins and corrins. Constraints are often applied either to accord with experimental data such as nOes, or to ensure the integrity of the simulations by constraining for example bond lengths to reasonable values (an instance of this is the widely-used SHAKE algorithm [306]). Some recent examples of the use of MD simulations in the chemistry of hemes and hemoproteins are considered below; the examples chosen are illustrative, rather than comprehensive.

3.3.2. Porphyrins and hemoprotein model compounds

Kollman and co-workers [307,308] have used MD simulations to investigate the differential binding of CO and O_2 by capped ferrous porphyrins. The calculations were performed with the AMBER force field and parameters for the ferrous porphyrin were determined empirically to model four known crystal structures of appropriate compounds [308]. The charges on the atoms were determined by an IEHT procedure for the porphyrin core, the metal and the CO or O_2 ligand, and, following AM1 [309,310] geometry optimization, by ab initio calculations at the STO3G level of theory using GAUSSIAN for the straps and pickets of the heme system. Charge neutrality was maintained by distributing excess charge to the protons of the porphyrin core. These calculations highlighted the importance of distal steric effects in discriminating in favor of bent coordination of O_2 as opposed to linear coordination of CO.

Quenched dynamics calculations involve the storing of structures during a dynamics run, sorting and identifying the lower energy structures, and then energy-minimizing. Such an approach is useful in exploring conformational space and in increasing the probability that a discovered minimum energy structure is the global minimum. An example of this is found in the study of Bruice and co-workers [194] on bridged cofacial metal-free tetraphenylporphyrin dimers using the CHARMm force field [150]. These workers were interested in finding an empirical correlation between the band width of electronic transitions of the porphyrin, and ^{1}H-74NMR signals of the pyrrolic N–H and other protons, with the interplanar distance of aza-bridged cofacial porphyrins. The strategy adopted was to perform long (100 ps) MD simulations at 600 K (after appropriate heating and equilibration phases); 2000 structures were collected during each dynamics run, the two lowest energy structures sought and energy-minimized. Reasonable agreement between the structures reached by this approach and known crystal structures of such compounds (inter-planar distances were reproduced to within 0.5 Å) increase confidence in the results obtained.

Dynamics simulations may be useful in exploring assumptions about molecular structure, and guiding synthesis endeavors. Frank and co-workers [311] have investigated the dynamics behavior of porphyrin–quinone complexes (Fig. 14) as a model for photo-induced electron transfer systems using the CFF91 force field; the force field is reported to reproduce well the crystal structures of such systems. It was assumed that the quinone moiety remains rigidly parallel to the porphyrin ring. However, the MD results showed that there is considerable motion in the porphyrin cap, and the plane of the quinone moiety tilts relative to the porphyrin, with the angle θ (Fig. 14), which should be close to 90° if the ring systems are co-planar, oscillating by about 120°, in a bimodal distribution with maxima at about 40 and 150°. Thus, there are two major populations; the first has one of the two carbonyls pointing downwards towards, and the other upwards away from the porphyrin.

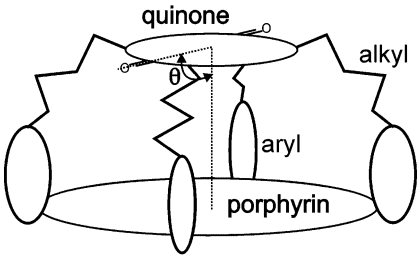

Fig. 14. A schematic representation of a porphyrin–quinone donor–acceptor system investigated as a photosynthesis model system. Alkyl = tetramethylene; aryl = phenyl, naphthyl, biphenylene. After Frank et al. [311].

There are limitations to molecular dynamics methods, of course. If one is interested in studying the interaction between molecules that are not covalently linked, the dynamics simulation may cause the molecules to fly apart, and no useful information is obtained. This limitation was found when studying the interaction between the antimalarial drug chloroquine and an iron porphyrin [265]. The way the problem was addressed was to generate a large number of initial structures, optimize each, group into equivalent structures, and sort. The structure with the lowest energy is then assumed to be a representative structure of the adduct between the two molecules. Essentially the same strategy has been used to investigate the interaction between the L and D isomers of tyrosine and a catalyst for its oxidation by H_2O_2, a chelated deuterohemin-glycyl-L-histidine complex [278] in an endeavor to explain the unexpected stereoselectivity of the oxidation reaction.

Miyamoto and co-workers [312] have used short (5–10 ps) MD simulations with the ESFF force field and the program MXDORTO [313] to investigate the interaction of Mg, Co and Fe porphyrins encapsulated in Y-type zeolites with the zeolite framework. The interest in this system stemmed from the possible use of porphyrins trapped in a host lattice as oxidation catalysts, the rationale being that the host lattice will protect the porphyrin from the reactions that can lead to its destruction. The zeolite structure will not allow two porphyrins to be close to each other; the system should therefore be protected against oxidative dimerization. They showed that provided the zeolite framework contains exchanged cations (such as sodium in NaY zeolite) to shield the metal from the framework oxygen atoms, the metal should be available for interaction with reactants.

3.3.3. The microperoxidases

Proteolytic digestion of cytochrome *c* leads to the formation of small hemepeptides, called microperoxidases, which retain the proximal His ligand of the parent protein (Fig. 15). The sixth (axial) coordination site is occupied by a water molecule [314,315]. These compounds have been extensively studied as models for the hemoproteins and in particular those hemoproteins that contain His as a proximal ligand [316,317]. To date, none of the microperoxidases have been successfully crystallized, but a number of groups have examined the structure by MD methods.

Ranghino and co-workers [318] began from the crystal structure of cytochrome *c*, and edited the protein to obtain MP-11, and energy-minimized using the CVFF force field and parameters listed in the paper for modeling the iron porphyrin. Details of the derivation of the parameters are not given, but the parameters appear to reproduce the essential features of ferric porphyrins

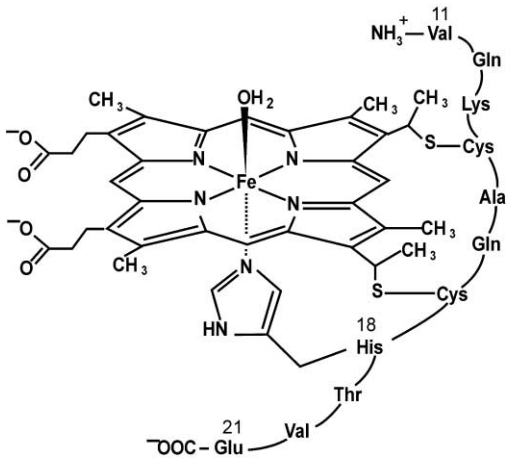

Fig. 15. The hemepeptides from cytochrome *c*. Microperoxidase-8 (MP-8) contains the residues Cys through Glu; MP-11 contains the residues shown. The residue numbering is based on the numbering of the parent protein.

reasonably well. Solvent was not included, but a distance-dependent dielectric constant was used. Molecular dynamics simulations were performed on this minimized structure, and a dimeric structure obtained from energy-minimizing random orientations of the two hemepeptides. The dimeric structure, studied to explore the nature of the aggregation MP-11 is known to undergo (see Ref. [319], and references therein), was embedded in a 9 Å layer of solvent water. The MD simulation of the monomer showed that the peptide is very flexible and generally randomly-coiled, except for the segment between the two Cys residues covalently linked to the porphyrin; this segment makes a half-helical turn and is held by an intra-chain hydrogen bond. The peptide is confined to the proximal face of the porphyrin and does not interact with the distal environment; hence, the N-terminus (on Val11) and the side chain of Lys13 cannot act as ligands *trans* to His18. In agreement with suggestions in the literature (see Ref. [319], and references therein), the formation of low-spin MP-11 that accompanies dimerization and higher aggregation must arise from inter-molecular coordination of the sixth coordination site of Fe(III). Although the MD modeling failed to show conclusive evidence for Fe–Lys intermolecular coordination, the Lys of one molecule does approach the Fe of the second quite closely. It is now known [319] that aggregation is due to intermolecular coordination either by the terminal amino group or the Lys side chain, since chemical blocking of these residues leads to a monomeric MP-11.

The solution structure of MP-11 has been addressed in detail by Melchionna and co-workers [320]. The starting structure in this study was also the parent cytochrome *c*, which was edited appropriately, and imidazole was coordinated in the sixth (axial) ligand position of the metal. Molecular dynamics simulations (100 ps) were conducted both in vacuo and in solvent water by using the uncharged (D) and charged (C) versions of the GROMOS force field [321]; in the latter simulation, water molecules were represented by a simple point charge (SPC) model. Interestingly, it was found that the presence of solvent led to a mean structure of MP-11 more closely related to the structure of the native protein. As expected, and as previously demonstrated by Ranghino et al. [318] (see above), the peptide showed greatest flexibility towards the end of the chain, away from the constraints imposed by the Cys linkages to the porphyrin. The portion of the protein between the Cys residues retains the semi-helical arrangement of the parent protein. Many hydrogen bonds between the side chains of the amino acid residues and the peptide backbone were identified and are probably responsible for maintaining the peptide chain localized on the proximal side of the porphyrin. As expected, the extent of hydrogen bonding within the peptide is significantly decreased in the presence of solvent.

In a follow-up study the same group used MD simulations to study the structure of MP-8 and MP-11 in aqueous and in a 4:1 MeOH:H_2O solvent system [322], where, for the latter system, a proton on water was replaced by a methyl group. It was found that in pure water solvent MP-11 has a conformation which is closer to the conformation of this fragment in the native protein; in mixed solvent the backbone is more stretched out with larger vibrational amplitudes of the atoms and the torsional angles of the peptide backbone. The aggregation of MP-11 and MP-8, studied by using two monomer units during the simulations, is consistent with a head-to-tail alignment and a stacked conformation, respectively. The hydrogen bonding network in the hemepeptides was examined in detail and in addition to intra-chain and chain-solvent hydrogen bonds, interactions were also discovered involving the heme propionates and the imidazole ring of the proximal His ligand.

3.3.4. Hemoglobin and myoglobin

Hemoglobin (Hb) and myoglobin (Mb), the oxygen carrier and storage proteins, respectively, of higher animals are amongst the best-studied of all proteins [10]; hence, it is not surprising to find that these proteins have been the subject of MD simulations. One of the limitations of MM methods is that bond breaking and bond making events are not readily studied because the force field parameters for the bonded and unbonded species are usually different. There are circumstances where this limitation can be circumvented. Thus, the structural changes that accompany the photodissociation of CO from ferrous Hb have been examined [323] using a relatively simple force field [324] that neglects electrostatic terms, although it does in-

clude a function for hydrogen bonding. The photodissociation process was simulated by interrupting a dynamics trajectory of the carbonyl complex of the α-chain of Hb and changing the potential function for the Fe–C bond to one in which there is no attractive interaction. Simultaneously, the parameters for Fe–N were changed from those that reproduce a six-coordinate heme with Fe in the plane to those that produce a domed five-coordinate iron porphyrin, as is seen in the structure of deoxyHb. To assess the effect of the protein, the study was repeated on the protein-free system, Fe(II)PPIX bonded to imidazole and CO. The half-life for the displacement of Fe from the mean porphyrin plane was in the 50–150 fs range for the protein and the isolated ferrous porphyrin, a result in agreement with the experimental observation that Fe is displaced from the porphyrin plane within 350 fs in both hemoglobin and a free heme complex in solution.

Nowak [325] has used molecular dynamics simulations to study the structural consequences of changes to the proximal ligand (His in the native protein) in human deoxyMb. His93(F8) was replaced by glycine, and the imidazole ring of the native ligand replaced by a series of substituted imidazoles and by pyridine. Hence, the covalent link between the proximal ligand and the protein is missing in these simulations. MD simulations were performed with MOIL [326], which uses features of the AMBER/OPLS and the CHARMm force field; default parameters in MOIL and the MOIL parameters of Czarnecka [327] were used for the porphyrin and for the new ligands, respectively. Despite the absence of the covalent link between the prosthetic group and the protein, the structure remains stable during the time course of the simulations (100 ps), and not very different to that of the wild type. The proximal ligand is found to be relatively flexible, and to adopt a range of conformations relative to the porphyrin ring. Surprisingly, many of the ligands adopt an eclipsed conformation relative to the porphyrin ring (i.e. the projection of the planar axial ligand onto the porphyrin plane eclipses, or nearly eclipses, a N_{porph}–Fe–N_{porph} vector). This is contrary to the known steric properties of porphyrins [162] and is clearly a consequence of the interaction of the proximal ligand with the protein environment; details are not given in the paper.

Kinetic data show there is an ca. 100 kJ mol^{-1} barrier to the separation of an iron porphyrin and a protein such as Hb, HRP and CCP (see Ref. [315], and references therein). Edholm et al. [328] have used MD simulations with the GROMOS force field [321] on myoglobin embedded in a periodic box of SPC water to study the release of the porphyrin. Since the time required for a spontaneous release is many orders of magnitude slower than can feasibly be studied at present using MD techniques, the authors resorted to a non-equilibrium study by applying a force to the porphyrin which eventually leads to its release within the timeframe of the simulations (hundreds of ps). An analysis of the time required for a given force to free the heme from the protein led to a prediction of an energy barrier of the correct order of magnitude. It was shown that the barrier is largely entropic, not enthalpic. Monitoring of the structural changes accompanying the release of the heme from the protein showed significant movement in the heme pocket, including the entering of Arg70 and some five water molecules into the pocket.

The structure of the distal environment of the heme pocket in carbonmonoxy myoglobin (MbCO) has been investigated with four independent 90 ps MD trajectories using the AMBER force field augmented with parameters for the heme group [329]. The trajectories revealed both an open and a closed heme pocket structure where, in the former, the distal histidine is displaced from the heme pocket. In the closed structures, the protonated N atom of the distal histidine, whether N_δ or N_ε, points into the heme pocket. This is in contrast to the neutron diffraction structure, but is consistent with the ν_{CO} stretching frequency of MbCO in solution.

3.3.5. The peroxidases

The catalases and peroxidases, or hydroperoxidases, are ferric hemoproteins that are oxidized by H_2O_2 to form compound I; this is a ferryl compound, Fe(IV) = O, with the other oxidizing equivalent located either on the porphyrin ring or on a protein residue. Compound I is either reduced by H_2O_2 itself (H_2O_2 disproportionation, the catalase reaction), or, by two one-electron transfers steps via compound II, by a substrate or a variety of redox partners (the peroxidase reaction) [19–21,330–332]. Crystal structures of beef liver catalase [333] and catalase HPII from *Escherichia coli* [25] and of several peroxidases (cytochrome *c* peroxidase (CCP) [334,335]; pea ascorbate peroxidase [336]; *Coprinus cinereus* peroxidase [337]; *Arthromices ramosus* peroxidase [338]; lignin peroxidase [339–341]; peanut peroxidase [342]; horseradish peroxidase [343]; manganese peroxidase [344], including the crystal structure of a complex between the electron transfer partners, CCP and cytochrome *c* [345]), are available. The peroxidase hemoproteins contain either His or Cys as an axial ligand. Where the proximal ligand is His, it is hydrogen bonded to an invariant Arg residue, and confers on the proximal ligand some imidazolate character which is important in stabilizing the higher oxidation state of the metal required during the catalytic cycle. Invariant distal His and Arg residues are important in the mechanism that leads to the formation of compound I [346,347]. A system of four water molecules are hydrogen bonded to residues in the distal pocket and are thought to be important in holding the distal residues in the correct orientation required for the initial interac-

tion with H_2O_2 that leads to the formation of compound I [335]. Two Ca^{2+} ions are required to maintain the structural integrity of the fungal and plant peroxidases [330,348–350].

MD calculations using the AMBER force field [147] have been performed [351,352] on structures beginning from the coordinates of CCP and lignin peroxides (LIP), including the crystallographically-discovered water molecules, and immersed in a 10 Å shell of TIP3P water molecules [353]. The porphyrin parameters used were those available for the modeling of these moieties [215,354–356]. Initial testing of the force field parameters showed that the structure of the heme active site was maintained very close to that observed crystallographically, which is consistent with available NMR evidence that the structure of these proteins in solution and in the solid state is very similar. For both proteins, the hydrogen bonding network between the ordered water molecules near the active site and protein residues was conserved during dynamics trajectories up to 160 ps (Fig. 16). The MD simulations confirmed the retention of a hydrophilic character in the distal environment, probably an important feature in the mechanism of the hydroperoxidase reactions, involving high oxidation states and charged intermediates. The presence of a water molecule (Fig. 16) throughout the dynamics trajectory, hydrogen bonded to the conserved proximal Asp235 residue, which in turn is hydrogen bonded to the proximal His175 ligand, is in accord with the suggestion that imparting imidazolate character to the proximal His may be an important feature in the mechanism of these proteins.

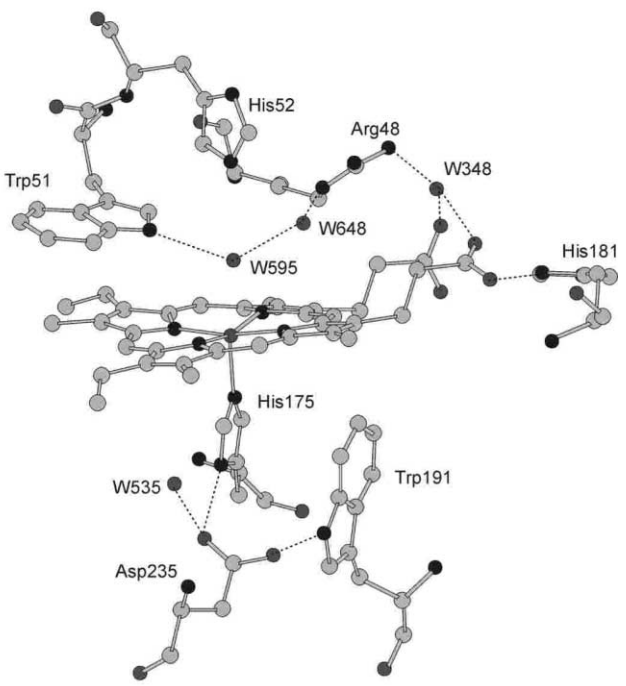

Fig. 16. The ordered water molecules and the hydrogen bonding network near the active site of CCP, conserved during molecular dynamics trajectories of up to 160 ps. (After Banci et al. [351]).

3.3.6. Cytochromes

The cytochromes *c* are electron transfer hemoproteins containing a *c*-type heme group, covalently linked from the periphery of the ring through Cys residues to the protein [357,358]. His and Met are the axial ligands of iron; the metal cycles between the $+2$ and $+3$ oxidation states as the protein relays electrons. Several MD simulations have been carried out. Simulations in bulk water have provided useful structural and dynamic information [359]. Other simulations have addressed the reorganization associated with electron transfer and showed that, in support of the concept of an entatic state, the reorganization energy in the protein is lower than for a naked heme in aqueous solution [360,361].

The structures of proteins from different organisms and in different oxidation states have been determined by both X-ray diffraction methods in the solid state and NMR methods in solution [362]. The significance of structural changes that appear to accompany a change in oxidation state, and apparent differences between the solid state and the solution structure is the cause of some debate [357]. In particular, the role of a water molecule (W166) in modulating the electron-withdrawing power of the axial Met ligand as it moves from 6.6 to 5.1 Å from the metal center on oxidation in yeast *iso*-I cytochrome *c* as deduced from the solid state structures [363,364] has been disputed; it has been suggested [365] that this is a characteristic feature of all eukaryotic cytochromes *c*. However, NMR studies on horse heart cytochrome *c* suggest that the position of W166 remains largely unchanged on oxidation of the protein [366].

Banci and co-workers [351] have simulated the dynamics trajectory of the reduced and oxidized forms of yeast *iso*-I cytochrome *c* immersed in solvent with long (600 ps) trajectories using the AMBER force field for the protein, and the previously derived parameters for the iron porphyrin. The charges on the porphyrin atoms were derived from ab initio calculations using a 6-31G* basis set for all atoms except the metal (which has handled with pseudo-potentials). They found, when starting from the coordinates of the oxidized and reduced forms, that W116 remains stable at ca. 7.8 Å from the metal in the oxidized protein, and migrated to this position in the reduced protein. The latter migration is accompanied by a shift in the position of the side chain of Tyr67, which creates a channel to the active site accessible by solvent molecules. Thus the MD simulations are in agreement with the NMR observations, and highlight some of the difficulties of deducing the structure and function of proteins from the solid

state structures; this is a caveat which, since the elucidation of the cooperativity mechanism of hemoglobin largely as a consequence of the solid state results, has not always been appreciated.

Simonson and Perahia [388] have performed a 1 ns MD simulation of yeast ferri-cytochrome *c* in TIP3P water [353] with the CHARMm/PARAm19 force field [150] to study the dielectric properties of the entire protein using linear response and thermodynamic perturbation theory. They calculated the relaxation free energies in response to a single test charge located on each successive C_α atom of the protein backbone. Protein and solvent contributions were found to be coupled and anti-correlated, so that the total relaxation free energy is smaller than either. The total relaxation free energy (due to electronic and dipolar contributions) increases smoothly by a factor of 2 as the test charge is moved from the protein center to its surface. Importantly, the prosthetic group is located in a region where relaxation is minimal, in agreement with the function of cytochrome *c* as an electron transfer protein, which necessarily requires that the reorganization energy that accompanies electron transfer to and from the metal ion is as small as possible.

Cytochrome b_5 participates in electron transfer in stearyl-CoA desaturation, and in the reduction of methemoglobin and cytochrome P450 [389]. There are two hydrophobic cores in the molecule, one of which binds the iron porphyrin. There is interest in the structure of the apoprotein since this is synthesized on the endoplasmic reticulum, whilst insertion of the iron porphyrin moiety occurs only later, in the mitochondria. There is considerable NMR information about the structure of rat apocytochrome b_5, but not of the bovine protein, and a crystal structure of bovine cytochrome b_5, but not of the rat protein. The structure of solvated rat and bovine apocytochrome b_5 has been investigated [390] by MD methods using the potential function of Levitt [324,391–393] and the program ENCAD [366]. The initial structure used was the crystal structure of the bovine protein with the heme removed. For the rat protein, six mutations were made, with the side chains of the new amino acids placed in approximately the same position as in the bovine protein. Work was first performed under conditions that simulated pH 2 (where the heme group is removed in vitro) for 200 ps by protonating the side chains of appropriate amino acids, and then under conditions that simulated pH 6.9 (1400 ps). The bovine protein simulation gave some inconsistencies with the experimental data on the rat protein—especially in the regions containing the variant amino acids—whereas simulations of the latter were in good agreement with the NMR data but showed marked differences to the crystal structure of the former. The hydrophobic core that normally contains the heme group (core 1) in the rat protein showed conformational heterogeneity, increased mobility, and some loss of secondary structure. The other hydrophobic core (core 2) maintained a native-like structure. Thus the MD work complements the NMR results, providing information about core 1 that has proved difficult to obtain by experimental methods. Moreover, the work provides a prediction of the solution structure of bovine apocytochrome b_5 not yet available experimentally.

The cytochromes P450 are a family of heme monooxygenases that catalyze the insertion of an oxygen atom into a C–H bond of the substrate, which may be a drug, a steroid, or a xenobiotic. Hydroxylation increases solubility and allows for removal of the xenobiotic from the cell [367]. Amongst the most widely studied P450s is the camphor hydroxylase ($P450_{cam}$) from *Pseudomonas putida*. Crystal structures are available for the substrate-free and substrate-bound forms [368,369]. As might be expected for a mono-oxygenase, the heme is well-shielded from the solvent and a comparison of the substrate-bound and substrate-free structures revealed no obvious pathway for substrate access to the active site. The protein must therefore be highly flexible and gate-opening motions must clearly be crucial during turnover. These sorts of questions can be probed by MD simulations.

Paulsen and Ornstein [370] used DISCOVER to model $P450_{cam}$ in a 175 ps MD simulation at 300 K; an all-atom model was used with the default parameters of the force field and the parameters of Giammona [371] for modeling the iron porphyrin. The 13 segments of α-helix and 5 segments of β-sheet were well preserved with the exception of one helix that alternated between an α- and a 3_{10}-helix. Two kinks in the crystal structure occur in two separate helices. These regions showed high mobility during the simulation. The kink in one of these helices, helix I, occurs at the oxygen binding site, and it is suggested that this may have functional implications. In particular, it was observed that Phe87 might adopt an alternate conformation resulting in a marked increase in the volume of the substrate-binding site. The protein may therefore accommodate significantly larger substrates than might have been anticipated from an examination of the crystal structure.

In a later study by the same authors [372], the structure of P450BM-3 from *Bacillus megaterium* was investigated. The protein catalyzes the oxidation of C14 to C20 fatty acids and contains an N-terminal heme-binding domain and a C-terminal reductase domain. The heme domain has been crystallized [373] and each asymmetric unit cell was found to contain two enzyme molecules which differ in their conformation about the substrate binding pocket, with molecule 1 having a more closed and less accessible substrate binding pocket than molecule 2. Since this difference could be a consequence of lattice forces, it was unclear whether the two

conformations are significantly populated in solution. This question was therefore investigated by separate 200 ps MD simulations of the two molecules embedded in solvent water. The differences in structures between the two molecules were preserved during the simulations, and the differences in the substrate binding sites of the two molecules diverge rather than converge. In particular, the mouth of the substrate-binding pocket was found to be highly mobile, which may be an important factor in allowing this enzyme to bind substrates of varying sizes. This point would not be readily apparent from an examination of the crystal structure alone.

These studies did not provide a clear answer about the substrate access channel in $P450_{cam}$. Wade and co-workers [374] used crystallographically determined temperature factors and thermal motion pathway analysis to identify possible access channels in the protein. At the same time, MD simulations using the CHARMm all-atom force field were performed in the protein embedded in TIP3P water. A force was applied to the protein-bound camphor molecule. If the camphor molecule did not move a given distance in a given time window, an alternative, randomly-chosen direction to the force was explored until the molecule reached the surface of the protein. The most likely pathway obtained from the thermal motion analysis could not be located by the MD simulation, but a pathway through a small opening above the active site which had previously been proposed as the substrate access channel from crystallographic data [368] was located by both methods. Good correspondence between the two methods was also found for an alternative pathway located along the F–G helices, the E-helix, and the E–F loop.

The cytochromes P450 provide an interesting example of the use of modeling as an adjunct to traditional methods of exploring structure. The crystal structures of four isozymes of bacterial origin ($P450_{cam}$, $P450_{terp}$, P450BM-3, and P450eryF) have been reported, but the structures of enzymes of mammalian forms have not yet been determined. Loew and co-workers [375] have developed protocols for the modeling of P450 structures; these are based on the known structure of the four P450s from bacterial sources. They include an improved procedure for sequence alignment of these proteins, the construction of the backbone either by copying the backbone coordinates in structurally conserved regions from the templates or by a loop search procedure for the unconserved regions, the generating of initial side chain conformations utilizing SA/Monte Carlo methods [376], and energy minimization of all but the backbone of the structurally conserved regions using the AMBER force field. Using the algorithm developed by Sippl [377], the interaction energy of each residue with the rest of the protein is then calculated based on a mean-field potential derived from known protein structures. Regions of high steric strain indicate either bad steric contact or misalignment, and the local structure is modified to correct the repulsive energy. Finally, an examination of the local hydrogen bonding network is made to add structurally-important water molecules. A set of rigorous criteria is then used to assess the quality of the model. The protocols were used to construct a model of rabbit liver microsomal P450 isozyme 2B4 and unconstrained MD simulations were performed with AMBER and parameters specifically developed for the heme moiety [378]. The model was found to be stable during these simulations and was used to identify the likely substrate access channel, the substrate binding site, and probable regions on the surface for binding with redox partners. A model of the human cytochrome P450 3A4 protein based on the known structure of the four bacterial P450s has been reported [379]. Although final energy minimization was performed in the presence of solvent, no MD simulation appears to have been attempted.

In addition to questions of structure, MD simulations may be useful to predict the oxidation products from P450-catalyzed oxidations. Some of the work in this area has been reviewed [380].

3.4. MD simulations: the solution structure of cobalt corrinoids

The solution structures of methylcobalamin (CH_3Cbl), methylcobinamide (CH_3Cbi^+), adenosylcobalamin (AdoCbl), adenosylcobinamide ($AdoCbi^+$), cyanocobalamin (CNCbl) and methyl-(3,5,6-trimethylbenzimidazolyl)cobamide (CH_3–[Me_3Bzm]Cba^+), an analog of base-off methylcobalamin in which the N3 position of the base is methylated, have been studied by molecular dynamics simulations [305,381,382]. Typically between 90 and 120 crosspeaks, not including those due to geminal hydrogens, could be resolved and assigned at the longest mixing time in the ROESY spectrum of each cobalt corrinoid. The assignments of the pro-chiral protons were made on a trial-and-error basis until the minimum number of violations of distance criteria was obtained during long (50–300 ps) simulations at 300 K. Any ambiguities in nOe assignments and strengths were also resolved during these simulations. After completion of this procedure, at most 10% (and often $< 5\%$) of H–H distances violated the distance criteria; this demonstrated that the MD-simulated structures were in good agreement with the experimental observations.

The consensus structure of each compound was found by a MD/SA annealing procedure, repeated 25 times for dynamics runs between 5 and 50 ps. After each simulation, the structure was energy minimized. Because AdoCbl exists in both a southern and an eastern conformation in solution at room temperature

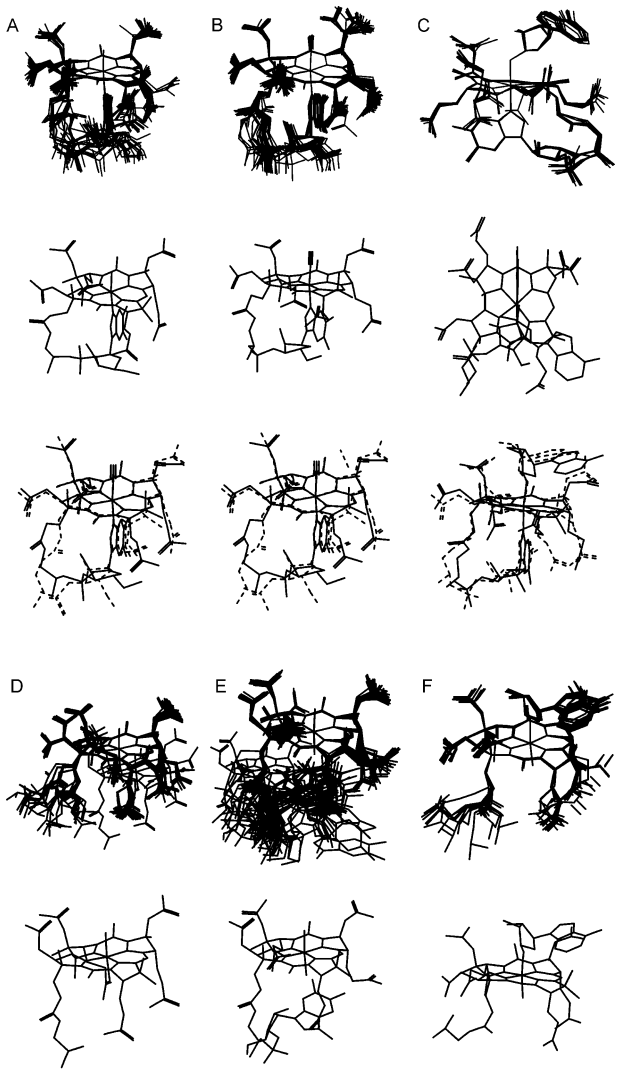

Fig. 17. The annealed structures overlaid at the N donor atoms of the corrin ring (top), the consensus structures (middle), and, for A, B and C (bottom), a comparison of the consensus structures (solid line) and the known crystal structures (broken line). A, MeCbl; B, CNCbl; C, AdoCbl (southern conformation); D, $MeCbi^+$; E, CH_3–[Me_3-Bzm]Cba^+; and F, $AdoCbi^+$ (southern conformation). Although 25 annealed structures were generated for each species, for clarity less are shown in some cases.

(see above), nOes arise that are due only to the southern conformation and to the eastern conformation, respectively. If the modeling is performed with all these nOes in position, the system responds by annealing into a compromise conformation between the southern and eastern conformations [382]; this is a clear misrepresentation of the structure of the molecule in solution. This problem was overcome by utilizing a two-state MD/SA procedure in which the nOes that arise from the eastern conformation only, and those that arise from the southern conformation only respectively, are omitted; this gives rise to annealed structures in, respectively, the southern and eastern conformations. The annealed structures were overlaid at the corrin N atoms and their coordinates averaged; energy minimization gave the average, or consensus structure. The overlaid structures and the consensus structures are illustrated in Fig. 17.

The consensus structures of CNCbl, CH_3Cbl and the southern conformation of AdoCbl are similar to the respective crystal structures, except for the disposition of the *f* side chain and the aminopropanol moiety of the nucleotide loop (Fig. 17). In most crystal structures, when the molecule is viewed from above in its standard orientation (Fig. 3), the C57–O58 carbonyl group points in a southeasterly direction, such that an extension of the C57–O58 vector would intersect an extension of the Co–C15 vector. This is referred to as the 'inward' conformation [161]. During MD simulations, the nucleotide loop spans a range of conformations from the 'inward' conformation to an 'outward' conformation, where the C57–O58 vector points away from the molecule in a southwesterly direction. Most structures anneal in this 'outward' conformation. At least one structure is known, 10-Cl–H_2OCbl (in which the C10 H of aquacobalamin has been replaced by Cl), where the molecule has crystallized in the 'outward' conformation [161]. The fold of the corrin ring (the angle between the mean planes through N21, C4, C5, C6, N22, C9, C10, and N24, C16, C15, C14, N23, C11, C10, respectively [118]) of the consensus structures agree well with those observed in the solid state: CNCbl (18.5° in the modeled structure [305]; 18.0° in the crystal structure (unpublished observations, C. Kratky)); CH_3Cbl (modeled, 16.8° [305]; solid state, 15.2° [383]); AdoCbl (modeled southern conformation, 13.5° [382]; solid state 13.3–14.8° [120,384]).

As mentioned, one of the advantages of a reliable MM force field is the ability to study the structures of compounds that fail to crystallize. Despite many attempts in many laboratories, neither an alkylcobinamide (a cobalt corrinoid containing an alkyl ligand in the upper or β coordination site, and in which the nucleotide loop has been chemically removed) or a base-off Cbl in which Bzm coordination of blocked (e.g. by methylation in the Me_3BzmCbas) has yet to be crystallized. The structures of two alkylcobinamides (methylcobinamide, CH_3Cbi^+; adenosylcobinamide, $AdoCbi^+$) and one Me_3BzmCba (methyl-(3,5,6-trimethyl-benzimidazolyl)cobamide, CH_3–[Me_3Bzm]Cba^+) have been studied [305,382]. The annealed structures and the consensus structure are shown in Fig. 17D–F.

The corrin fold angles are smaller than in the cobalamins. CH_3Cbi^+ has a fold angle of 13.1° (the average of the 25 annealed structures was 12.3°, with 9.5° min and 16.0° max); the southern conformation of $AdoCbi^+$ has a fold angle of 9.9° (average of the 25

structures, 13.9°, 3.3° min, 13.8° max); whilst CH_3–[Me_3Bzm]Cba$^+$ has a fold angle of 9.2° (average 8.5°, 3.4° min, 11.8° max) [305,382]. There is crystallographic evidence [305] that the corrin fold angle is greater in the cobalamins than in the cobinamides. Since the absence of the base in the α position of a cobalamin allows for a more planar structure, this suggests that base-on cobalamins are under steric strain. These observations lend support to suggestions [289,294–296,385–387] that the corrin fold may be an important factor in explaining why alkylcobalamins are more reactive towards Co–C bond homolysis than alkylcobinamides. The flexing of the corrin may have implications for the mechanism of enzymatic activation of Co–C bond activation [287–290] (see Section 3.2.1).

4. Summary

Despite its limitations, MM remains a computationally-efficient and (provided sufficient care is taken in the derivation of the appropriate force field parameters) reliable method for exploring the structures of even relatively complex molecules such as the porphyrins and the corrins. The quality force fields available for both these classes of molecules make MM techniques very valuable tools in research endeavors in these areas.

5. Nomenclature

AdePrCbl	adeninylpropylcobalamin
AdoCbl	5′-deoxyadenosylcobalamin (coenzyme B_{12})
Bzm	5,6-dimethylbenzimidazole, the base in intact cobalamins
$BzNH_2$	benzylamine
1-$BuNH_2$	1-butylamine
Cbi	cobinamide
Cbl	cobalamin
CCP	cytochrome *c* peroxidase
CH_3Cbl	methylcobalamin
CH_3-[Me_3Bzm]-Cba$^+$	methyl-(3,5,6-trimethylbenzimidazolyl)cobamide
CNCbl	cyanocobalamin (vitamin B_{12})
CSD	Cambridge Structural Database
Ct	centroid of the porphyrin in the mean porphyrin plane
DAP	3,5,7,13,15,17-hexaethyl-2,8,12,18-tetramethylporphyrin
deoxyMb	deoxymyoglobin
R- and *S*-DHPrCbl	*R*- and *S*-dihydroxypropylcobalamin
DPP	2,3,5,7,8,10,12,13,15,17,18,20-dodecaphenylporphyrin
Fe(II)PPIX	ferrous protoporphyrin IX
$[Fe(OEP)]_2O$	(μ-oxo)bis[(octaethylporphinato)-iron(III)]
$H_2T(n\text{-}N\text{-}MPy)P$	tetrakis(*n*-*N*-methylpyridyl)porphyrin; $n = 2, 3, 4$
Hb	hemoglobin
HRP	horseradish peroxidase
IEHT	iterative extended Hückel theory
Mb	myoglobin
MbCO	carbonmonoxy myoglobin
MD	molecular dynamics
MeCbl	methyl cobalamin
1-MeIm	1-methylimidazole
2-MeHIm	2-methylimidazole
1,2-Me_2Im	1,2-dimethylimidazole
MM	molecular mechanics
NPhPPDME	*N*-phenylprotoporphyrin IX dimethyl ester
nOe	nuclear Overhauser enhancement
OEP	octaethylporphyrin
OETPP	2,3,7,8,12,13,17,18-octaethyl-5,10,15,20-tetraphenylporphyrin
OMTPP	2,3,7,8,12,13,17,18-octamethyl-5,10,15,20-tetraphenylporphyrin
OPTPP	2,3,7,8,12,13,17,18-octapropyl-5,10,15,20-tetraphenylporphyrin
ROESY	rotating-frame Overhauser enhancement spectroscopy
SA	simulated annealing
SPC	simple point charge
T′BuP	5,10,15,20-tetra(*t*-butyl)porphyrin
TC_nTPP	($n = 5, 6, 7$); 2,3,7,8,12,13,17,18-tetracyclo(pent, hex, hept)enyl-5,10,15,20-tetraphenylporphyrin
TC_5TEP	2,3,7,8,12,13,17,18-tetracyclopentenyl-5,10,15,20-tetraethylporphyrin
TC_5TMP	2,3,7,8,12,13,17,18-tetracyclopentenyl-5,10,15,20-tetramethylporphyrin
TC_5TPtP	2,3,7,8,12,13,17,18-tetracyclopentenyl-5,10,15,20-tetrapentylporphyrin
$TC_5T(3,4,5\text{-}OMe)P$	2,3,7,8,12,13,17,18-tetracyclopentenyl-5,10,15,20-tetrakis(3,4,5-trimethoxyl)-phenylporphyrin
TFP	5,10,15,20-tetra(*ortho*-difluoro)-phenylporphyrin
TClP	5,10,15,20-tetra(*ortho*-dichloro)-phenylporphyrin
$T\text{-}2,6\text{-}(OH)_2\text{-}PP$	5,10,15,20-tetra(2,6-dihydroxy)-phenylporphyrin
$T\text{-}2,6\text{-}(X)_2PP$	5,10,15,20-tetra(2,6-dihalo)-phenylporphyrin; X = fluoro, chloro
TMP	5,10,15,20-tetramesitylporphyrin
TPP	5,10,15,20-tetraphenylporphyrin
TPrP	5,10,15,20-tetra-*n*-propylporphyrin

Acknowledgements

The financial assistance of the University of the Witwatersrand, through the Molecular Sciences Institute, and the National Research Foundation, Pretoria (H.M.M.) and the National Institute of General Medical Sciences, Grant GM48858 (K.L.B.) is gratefully acknowledged. Dr O.Q. Munro (University of Natal, Pietermaritzburg, South Africa) is thanked for helpful discussions.

References

[1] D.H. Andrews, Phys. Rev. 36 (1930) 544.
[2] I. Dostrovsky, E.D. Hughes, C.K. Ingold, J. Chem. Soc. (1946) 173.
[3] T.L. Hill, J. Chem. Phys. 14 (1946) 465.
[4] F.H. Westheimer, J.E. Mayer, J. Chem. Phys. 14 (1946) 733.
[5] J.C.A. Boeyens, Struct. Bonding (Berlin) 63 (1985) 64.
[6] J.C.A. Boeyens, P. Comba, Coord. Chem. Rev. 212 (2001) 3.
[7] D. Dolphin (Ed.), The Porphyrins, Academic Press, New York, 1978.
[8] K.N. Kadish, K.M. Smith, R. Guilard, The Porphyrin Handbook, Academic Press, San Diego, CA, 2000.
[9] M.F. Perutz, G. Fermi, B. Luisi, B. Shaanan, R.C. Liddington, Acc. Chem. Res. 20 (1987) 309.
[10] M.F. Perutz, Mechanisms of Cooperativity and Allosteric Regulation in Proteins, Cambridge University Press, Cambridge, UK, 1990.
[11] J.P. Collman, L. Fu, Acc. Chem. Res. 32 (1999) 455.
[12] R. Gennis, S. Ferguson-Miller, Science 269 (1995) 1063.
[13] S.M. Musser, M.H.B. Stowell, S.I. Chan, Adv. Enzymol. Rel. Areas Mol. Biol. 71 (1995) 79.
[14] B.G. Malmstr'm, J. Biol. Inorg. Chem. 3 (1998) 339.
[15] J.H. Dawson, Science 240 (1988) 433.
[16] J.A. Alberta, L.A. Andersson, J.H. Dawson, J. Biol. Chem. 264 (1989) 20467.
[17] L. Weber, G. Haufe, Z. Chem. 29 (1989) 88.
[18] T.L. Poulos, R.E. Fenna, Metal Ions Biol. Syst. 30 (1994) 25.
[19] G. Smulevich, Biochem. Soc. Trans. 23 (1995) 240.
[20] A.M. English, G. Tsaprailis, Adv. Inorg. Chem. 43 (1995) 79.
[21] R.W. Estarbrook, FASEB J. 10 (1996) 202.
[22] H. Dalton, P. Wilkins, Biochem. Soc. Trans. 25 (1997) 69.
[23] L. Banci, J. Biotechnol. 53 (1997) 253.
[24] I.S. Issac, J.H. Dawson, Essays Biochem. 34 (1999) 51.
[25] J. Bravo, N. Verdaguer, J. Tomo, C. Betzel, J. Switala, P. Loewen, J. Fita, Structure 3 (1995) 491.
[26] P. Loewen, Cold Spring Harbor Monogr. Ser. 34 (1997) 273.
[27] H. Ruis, F. Koller, Cold Spring Harbor Monogr. Ser. 34 (1997) 309.
[28] J. Bravo, I. Fita, P. Gouet, H.M. Jouve, W. Melik-Adamyan, G.N. Murshudov, Cold Spring Harbor Monogr. Ser. 34 (1997) 407.
[29] S.G. Boxer, Biochim. Biophys. Acta 726 (1983) 265.
[30] P.F. Lindley, Rep. Prog. Phys. 59 (1996) 867.
[31] M. Luebben, Biochim. Biophys. Acta 1229 (1995) 1.
[32] V.L. Davidson, Acc. Chem. Res. 33 (2000) 87.
[33] T. Yamazaki, H. Oyanagi, T. Fujiwara, Y. Fukumori, Eur. J. Biochem. 233 (1995) 665.
[34] B.R. Crane, L.M. Siegel, E.D. Getzoff, Biochemistry 36 (1997) 12101.
[35] W.R. Scheidt, Y.J. Lee, Struct. Bonding (Berlin) 1 (1987) 64.
[36] W. Jentzen, M.C. Simpson, J.D. Hobbs, X. Song, T. Ema, N.Y. Nelson, C.J. Medforth, K.M. Smith, M. Veyrat, M. Mazzanti, R. Ramasseul, J.-C. Marchon, T. Takeuchi, W.A. Goddard, J.A. Shelnutt, J. Am. Chem. Soc. 117 (1995) 11085.
[37] R.G. Alden, M.R. Ondrias, J.A. Shelnutt, J. Am. Chem. Soc. 112 (1990) 691.
[38] S. Franzen, J.C. Lambry, B. Bohn, C. Poyart, J.L. Martin, Nat. Struct. Biol. 1 (1994) 230.
[39] S. Franzen, B. Bohn, C. Poyart, J.L. Martin, Biochemistry 34 (1995) 1224.
[40] J.D. Hobbs, J.A. Shelnutt, J. Protein Chem. 14 (1995) 19.
[41] W. Jentzen, Y.-Z. Song, J.A. Shelnutt, J. Phys. Chem. B 101 (1997) 1684.
[42] W. Jentzen, J.-G. Ma, J.A. Shelnutt, Biophys. J. 74 (1998) 753.
[43] L.R. Furnelid, M.W. Renner, K.M. Smith, J. Fajer, J. Am. Chem. Soc. 112 (1990) 1634.
[44] L.R. Furnelid, M.W. Renner, J. Fajer, J. Am. Chem. Soc. 112 (1990) 8987.
[45] D.E. Trourud, M.F. Schmid, B.W. Matthews, J. Mol. Biol. 188 (1986) 443.
[46] M.O. Senge, J. Photochem. Photobiol. B16 (1992) 3.
[47] J. Deisenhofer, H. Michel, Angew. Chem. Int. Ed. Engl. 28 (1989) 829.
[48] J.A. Shelnutt, X.-Z. Song, J.-G. Ma, S.-L. Jia, W. Jentzen, C.J. Medforth, Chem. Soc. Rev. 27 (1998) 31.
[49] K.M. Barkigia, M.D. Berber, J. Fajer, C.J. Medforth, W.M. Renner, K.M. Smith, J. Am. Chem. Soc. 112 (1990) 8851.
[50] M. Ravikanth, D. Reddy, A. Misra, T.K. Chandrashekar, K. Tavarakere, J. Chem. Soc. Dalton Trans. (1993) 1137.
[51] M.O. Senge, T. Ema, K.M. Smith, J. Chem. Soc. Chem. Commun. (1995) 733.
[52] J. Takeda, M. Sato, Chem. Lett. (1995) 939.
[53] M. Veyrat, R. Ramasseul, J.-C. Marchon, I. Turowska-Tyrk, W.R. Scheidt, New J. Chem. 19 (1995) 1199.
[54] R.-J. Cheng, P.-Y. Chen, G. Ping-Yu, P.-R. Gau, C.-C. Chen, S.-M. Peng, J. Am. Chem. Soc. 119 (1997) 2563.
[55] M.O. Senge, C.J. Medforth, T.P. Forsyth, D.A. Lee, M.M. Olmstead, W. Jentzen, R.K. Pandey, J.A. Shelnuttt, K.M. Smith, Inorg. Chem. 36 (1997) 1149.
[56] M. Nakamura, T. Ikeue, H. Fujii, T. Yoshimura, J. Am. Chem. Soc. 119 (1997) 6284.
[57] M. Grodzicki, H. Flint, H. Winkler, F.A. Walker, A.X. Trautwein, J. Phys. Chem. A 101 (1997) 4202.
[58] H. Duval, V. Bulach, J. Fischer, M.W. Renner, J. Fajer, R. Weiss, J. Biol. Inorg. Chem. 2 (1997) 66.
[59] M.O. Senge, W.W. Kalisch, Inorg. Chem. 36 (1997) 6103.
[60] J.-Y. Zheng, K. Konishi, T. Aida, Inorg. Chem. 37 (1998) 2591.
[61] M.O. Senge, M.W. Reamer, W.W. Kalisch, J. Fajer, J. Chem. Soc. Dalton Trans. (2000) 381.
[62] C.J. Medforth, M.D. Barber, K.M. Smith, J.A. Shelnutt, Tetrahedron Lett. 31 (1990) 3719.
[63] J.A. Shelnutt, C.J. Medforth, M.D. Berber, K.M. Barkigia, K.M. Smith, J. Am. Chem. Soc. 113 (1991) 4077.
[64] A.B.J. Parusel, T. Wondbnagegu, A. Ghosh, J. Am. Chem. Soc. 122 (2000) 6371.
[65] D. Melamed, T.G. Spiro, J. Phys. Chem. 97 (1993) 7441.
[66] R.-J. Cheng, P.-Y. Chen, Chem. Eur. J. 5 (1999) 1708.
[67] A.I. Scott, B. Yagen, E. Lee, J. Am. Chem. Soc. 95 (1973) 5761.
[68] A.R. Battersby, M. Ihara, E. McDonald, F. Satoh, D.C. Williams, Chem. Commun. (1975) 436.
[69] A.R. Battersby, E. McDonald, R. Hollenstein, M. Ihara, F. Satoh, D.C. Williams, J. Chem. Soc. Perkin I (1977) 166.
[70] K. Bernhauer, F. Wagner, Biochem. Z. 335 (1962) 453.
[71] R.A. Ronzio, H.A. Barker, Biochemistry 6 (1967) 2344.
[72] X. Zou, D.R. Evans, K.L. Brown, Inorg. Chem. 34 (1995) 1634.
[73] P. Renz, Biochem. Biophys. Res. Commun. 30 (1968) 373.

[74] P. Renz, Methods Enzymol. 18C (1971) 82.
[75] W. Friedrich, K. Bernhauer, Chem. Ber. 89 (1956) 2030.
[76] K.L. Brown, G.-Z. Wu, Organometallics 12 (1993) 496.
[77] R.T. Taylor, in: D. Dolphin (Ed.), B_{12}, vol. 2, Wiley, New York, 1982 chapter 12.
[78] C.L. Drennan, R.G. Matthews, M.L. Ludwig, Curr. Opinion Struct. Biol. 4 (1994a) 919.
[79] R.G. Matthews, in: R. Banerjee (Ed.), Chemistry and Biochemistry of B12, Wiley, New York, 1999, p. 681.
[80] L.G. Ljungdahl, H.G. Wood, in: D. Dolphin (Ed.), B_{12}, vol. 2, Wiley, New York, 1982 chapter 7.
[81] H.G. Wood, S.W. Ragsdale, E. Pezacka, Trends Biochem. Sci. 11 (1986) 14.
[82] R.K. Thauer, Eur. J. Biochem. 176 (1988) 497.
[83] S.W. Ragsdale, Crit. Rev. Biochem. Mol. Biol. 26 (1991) 261.
[84] S.W. Ragsdale, in: R. Banerjee (Ed.), Chemistry and Biochemistry of B12, Wiley, New York, 1999, p. 633.
[85] E.N.G. Marsh, Essays Biochem. 34 (1999) 139.
[86] M. Fontecave, E. Mulliez, in: R. Banerjee (Ed.), Chemistry and Biochemistry of B12, Wiley, New York, 1999, p. 731.
[87] C.C. Lawrence, J. Stubbe, Curr. Opin. Chem. Biol. 2 (1998) 650.
[88] B.P. Hay, R.G. Finke, J. Am. Chem. Soc. 108 (1986) 4820.
[89] K.L. Brown, J. Li, J. Am. Chem. Soc. 120 (1998) 9466.
[90] W. Buckel, B.J. Golding, Chem. Soc. Rev. (1996) 329.
[91] B.T. Golding, W. Buckel, in: M.L. Sinnott (Ed.), Comprehensive Biological Catalysis, Academic Press, London, 1997, p. 239.
[92] R. Padmakumar, S. Taoke, R. Padmakumar, R. Banerjee, J. Am. Chem. Soc. 117 (1995) 7033.
[93] O. Zelder, B. Beatrix, F. Kroll, W. Buckel, FEBS Lett. 369 (1995) 252.
[94] F. Mancia, N.H. Keep, A. Nakagawa, P.F. Leadlay, S. McSweeney, B. Rasmussen, P. Bösecke, O. Diat, P.R. Evans, Structure 4 (1996) 339.
[95] N.H. Thomä, T.W. Meier, P.R. Evans, P.F. Leadley, Biochemistry 37 (1998) 14386\.
[96] F. Mancia, P.R. Evans, Structure 6 (1998) 711.
[97] R. Reitzer, K. Grhber, G. Jogl, V.G. Wagner, H. Bothe, W. Buckel, C. Kratky, Structure 7 (1999) 891.
[98] C.L. Drennan, S. Huang, J.T. Drummond, R.G. Matthews, M.L. Ludwig, Science 266 (1994) 1669.
[99] M.L. Ludwig, R.G. Matthews, Annu. Rev. Biochem. 66 (1997) 269.
[100] M. Yamanishi, S. Yamada, H. Muguruma, Y. Murakami, T. Tobimatsu, A. Ishida, J. Yamauchi, T. Toraya, Biochemistry 37 (1998) 4799.
[101] A. Abend, R. Nitsche, V. Bandavian, E. Stupperich, J. Rétey, Angew. Chem. Int. Ed. 37 (1998) 625.
[102] C.C. Lawrence, G.J. Gerfen, V. Samano, R. Nitsche, M.J. Robins, J. Rétey, J. Stubbe, J. Biol. Chem. 274 (1999) 7039.
[103] T. Tobimatsu, T. Hara, M. Sakaguchi, Y. Kishimoto, Y. Wada, M. Sakai, T. Toraya, J. Biol. Chem. 270 (1995) 7142.
[104] T. Tobimatsu, M. Azuma, H. Matsubara, H. Takatovi, T. Niida, K. Nishimoto, H. Satoh, R. Hayashi, T. Toraya, J. Biol. Chem. 271 (1996) 22352.
[105] L.R.P. Faust, J.A. Connor, D.M. Roof, J.A. Hoch, B.M. Babior, J. Biol. Chem. 265 (1990) 12462.
[106] S.B. Booker, J. Stubbe, Proc. Natl. Acad. Sci. USA 90 (1993) 8352.
[107] N. Shibata, J. Masuda, T. Tobimatsu, T. Toraya, K. Suto, Y. Morimoto, N. Yasuoka, Structure 7 (1999) 997.
[108] N. Shibata, J. Masuda, T. Tobimatsu, T. Toraya, K. Sato, Y. Morimoto, N. Yasuoka, Structure 7 (1999) 997.
[109] G.N. Sando, R.L. Blakley, H.P.C. Hogenkamp, P.T. Hoffmann, J. Biol. Chem. 250 (1975) 8774.
[110] M.I. Yakusheva, A.A. Poznanskaya, T.A. Pospelova, I.P. Rudakova, A.M. Yurkevich, V.A. Yakovlev, Biochim. Biophys. Acta 484 (1977) 216.
[111] T. Toraya, in: B. Kräutler, D. Arigone, B.T. Golding (Eds.), Vitamin B12 and B12-Proteins, VCH, Weinheim, 1998, p. 303.
[112] H. Bothe, G. Bröker, U. Müller, I. Schall, S. Textor, B.T. Golding, W. Buckel, in: B. Kräutler, D. Arigone, B.T. Golding (Eds.), Vitamin B12 and B12 Proteins, VCH, Weinheim, 1998, p. 237.
[113] W. Buckel, G. Broker, H. Bothe, A.J. Pierik, B.T. Golding, in: R. Banerjee (Ed.), Chemistry and Biochemistry of B12, Wiley, New York, 1999, p. 757.
[114] D.C. Hodgkin, J. Pickworth, J.H. Robinson, K.N. Trueblood, R.J. Prosen, J.G. White, Nature (London) 176 (1956) 325.
[115] D.C. Hodgkin, J. Kamper, M. Mackay, M. Pickworth, K.N. Trueblood, J.G. White, Nature (London) 178 (1956) 64.
[116] P.G. Lenhert, D.C. Hodgkin, Nature (London) 194 (1962) 1175.
[117] P.G. Lenhert, Proc. R. Soc. London A303 (1968) 45.
[118] J.P. Glusker, in: D. Dolphin (Ed.), B_{12}, vol. 1, Wiley, New York, 1982 chapter 3.
[119] K. Gruber, G. Jogl, G. Klintschar, C. Kratky, in: B. Kräutler, D. Arigone, B.T. Golding (Eds.), Vitamin B12 and B12-Proteins, VCH, Weinheim, 1998, p. 335.
[120] H.F.J. Savage, P.F. Lindley, J.L. Finney, P.A. Timmons, Acta Crystallogr. Sect. B 43 (1987) 280.
[121] I. Sagi, M.D. Wirt, E. Chen, S. Frisbie, M.R. Chance, J. Am. Chem. Soc. 112 (1990) 8639.
[122] M.D. Wirt, I. Sagi, S.M. Frisbie, R. Lee, M.R. Chance, J. Am. Chem. Soc. 113 (1991) 5299.
[123] M.D. Wirt, I. Sagi, M.R. Chance, Biophys. J. 63 (1992) 412.
[124] I. Sagi, M.R. Chance, J. Am. Chem. Soc. 114 (1992) 8061.
[125] E.M. Scheuring, I. Sagi, M.R. Chance, Biochemistry 33 (1994) 6310.
[126] S.M. Frisbie, M.R. Chance, Biochemistry 32 (1993) 13886.
[127] M.D. Wirt, M. Kumar, S.W. Ragsdale, M.R. Chance, J. Am. Chem. Soc. 115 (1993) 2146.
[128] E.M. Scheuring, R. Padmakumar, R. Banerjee, M.R. Chance, J. Am. Chem. Soc. 119 (1997) 12192.
[129] C. Kratky, G. Fäber, K. Gruber, K. Wilson, Z. Dauter, H.F. Nolting, R. Konrat, B. Kräutler, J. Am. Chem. Soc. 117 (1995) 4654.
[130] M. Tollinger, R. Konrat, B.H. Hilbert, E.N.G. Marsh, B. Kräutler, Structure (London) 6 (1998) 1021.
[131] G.R. Brubaker, D.W. Johnson, Coord. Chem. Rev. 53 (1984) 1.
[132] R.D. Hancock, Progr. Inorg. Chem. 37 (1989) 189.
[133] B.P. Hay, Coord. Chem. Rev. 126 (1993) 177.
[134] P. Comba, Coord. Chem. Rev. 123 (1993) 1.
[135] M. Zimmer, Chem. Rev. 95 (1995) 2629.
[136] P. Comba, T.W. Hambley, Molecular Modeling of Inorganic Compounds, VCH, Weinheim, 1995.
[137] J.A. Shelnutt, in: K.M. Kadish, K.M. Smith, R. Guilard (Eds.), The Porphyrin Handbook, vol. 7, Academic Press, San Diego, 2000, p. 167.
[138] J.P. Bowen, N.L. Allinger, in: K.B. Lipkowitz, D.B. Boyd (Eds.), Reviews in Computational Chemistry, vol. 2, VCH, New York, 1991, p. 81 chapter 3.
[139] N.L. Allinger, Adv. Phys. Org. Chem. 13 (1976) 1.
[140] N.L. Allinger, J. Am. Chem. Soc. 99 (1977) 8127.
[141] N.L. Allinger, Y. Yuh, MM2(87). Distributed to academic users by the Quantum Chemistry Program Exchange (QCPE), under special agreement with Molecular Design Ltd., San Leandro, CA.
[142] N.L. Allinger, Y.H. Yuh, J.-H. Lii, J. Am. Chem. Soc. 111 (1989) 8551.
[143] N.L. Allinger, MM3(92), QCPE, Bloomington, IN, 1992.

[144] N.L. Allinger, X. Zhou, J. Bergsma, J. Mol. Struct. (Theochem.) 312 (1994) 69.
[145] W.L. Jorgensen, J. Tirado-Rives, J. Am. Chem. Soc. 110 (1988) 1657.
[146] J. Pranate, S. Wierschke, W.L. Jorgensen, J. Am. Chem. Soc. 113 (1991) 2810.
[147] S.J. Weiner, P.A. Kollman, D.A. Case, U.C. Singh, C. Ghio, G. Alagona, S. Profeta, J. Am. Chem. Soc. 106 (1984) 765.
[148] S.J. Weiner, P.A. Kollman, D.T. Nguyen, D.A. Case, J. Comput. Chem. 7 (1986) 230.
[149] W.D. Cornell, Cieplak, C.J. Bayly, I.R. Gould, K.M. Merz, D.M. Ferguson, D.C. Spellmeyer, T. Fox, J.W. Caldwell, P.A. Kollman, J. Am. Chem. Soc. 117 (1995) 5179.
[150] B.R. Brooks, R.E. Bruccoleri, B.D. Olafson, D.J. States, S. Swaminathan, M. Karplus, J. Comput. Chem. 4 (1983) 187.
[151] M.S. Bovill, D.J. Chadwick, I.O. Sutherland, J. Chem. Soc. Perkin Trans. 2 (1980) 1529.
[152] A. Vedani, M. Dobler, J.D. Dunitz, J. Comput. Chem. 7 (1986) 701.
[153] M.D. Adams, P.W. Wade, R.D. Hancock, Talanta 37 (1990) 875.
[154] G. Wipff, P. Weiner, P. Kollman, J. Am. Chem. Soc. 104 (1982) 3249.
[155] P. Kollman, G. Wipff, U.C. Singh, J. Am. Chem. Soc. 107 (1985) 2212.
[156] A. Vedani, D. Huhta, S.P. Jacobsen, J. Am. Chem. Soc. 111 (1989) 4075.
[157] L.J. Bartolotti, L.G. Dederson, P.S. Charifson, J. Comput. Chem. 12 (1991) 1125.
[158] J. Mullay, J. Comput. Chem. 12 (1991) 369.
[159] P. Cieplak, P. Kollman, J. Comput. Chem. 12 (1991) 1232.
[160] S.L. Price, C.H. Faerman, C.W. Murray, J. Comput. Chem. 12 (1991) 1187.
[161] K.L. Brown, S. Cheng, X. Zou, J.D. Zubkowski, E.J. Valente, L. Knapton, H.M. Marques, Inorg. Chem. 36 (1997) 3666.
[162] O.Q. Munro, J.C. Bradley, R.D. Hancock, H.M. Marques, F. Marsicano, P.W. Wade, J. Am. Chem. Soc. 114 (1992) 7218.
[163] M.O. Senge, C.J. Medforth, L.D. Sparks, J.A. Shelnutt, K.M. Smith, Inorg. Chem. 32 (1993) 1716.
[164] O.Q. Munro, H.M. Marques, P.G. Debrunner, K. Mohanrao, W.R. Scheidt, J. Am. Chem. Soc. 117 (1995) 935.
[165] H.M. Marques, O.Q. Munro, N.E. Grimmer, D.C. Levendis, F. Marsicano, T. Markoulides, J. Chem. Soc. Faraday Trans. 91 (1995) 1741.
[166] B. Cheng, O.Q. Munro, H.M. Marques, W.R. Scheidt, J. Am. Chem. Soc. 119 (1997) 10726.
[167] S. Fitzwater, L.S. Bartell, J. Am. Chem. Soc. 98 (1976) 5107.
[168] P. Comba, Coord. Chem. Rev. 182 (1999) 343.
[169] A. Rappé, C.J. Casewit, K.S. Colwell, W.A. Goddard, W.M. Skiff, J. Am. Chem. Soc. 114 (1992) 10024.
[170] J.M. Sirovatka, A. Rappe, R.G. Finke, Inorg. Chim. Acta 300–302 (2000) 545.
[171] P. Comba, T.W. Hambley, N. Okon, N. MOMEC, a molecular modeling package for inorganic compounds, Altenhoff & Schmitz, Dortmund, Germany, 1995.
[172] V.S. Allured, C.M. Kelley, C.R. Landis, J. Am. Chem. Soc. 113 (1991) 1.
[173] R.J. Deeth, Coord. Chem. Rev. 212 (2001) 11.
[174] E. Unger, R.J. Lipski, W. Dreybridt, R. Schweitzer-Stenner, J. Raman Spectrosc. 30 (1999) 3.
[175] E. Unger, M. Beck, R.J. Lipski, W. Dreybrodt, C.J. Medforth, K.M. Smith, R. Schweitzer-Stenner, J. Phys. Chem. B 103 (1999) 10022.
[176] J. Gao, in: P.v.R. Schleyer (Ed.), Encyclopedia of Computational Chemistry, vol. 2, Wiley, Chichester, 1998, p. 1244.
[177] K.M. Merz, R.V. Stanton, in: P.v.R. Schleyer (Ed.), Encyclopedia of Computational Chemistry, vol. 4, Wiley, Chichester, 1998, p. 2330.
[178] D.S. Hartsough, K.M. Merz, J. Phys. Chem. 99 (1995) 11266.
[179] I.B. Berusker, M.K. Leong, J.E. Boggs, R.S. Pearlman, Bol. Soc. Chil. Quim. 42 (1997) 405.
[180] M. Clark, R.D. Cramer, N. Van Opdenbosch, J. Comput. Chem. 10 (1989) 982.
[181] B. Kräutler, R. Konrat, E. Stuppenrich, G. Farber, K. Gruber, C. Kratky, Inorg. Chem. 33 (1994) 4128.
[182] F. Maseras, New J. Chem. (1998) 327.
[183] M.J. Frisch, G.W. Trucks, H.B. Schlegel, P.M.W. Gill, B.G. Johnson, M.W. Womg, J.B. Foresman, M.A. Robb, M. Head-Gordon, E.S. Replogle, R. Gomperts, J.L. Andreas, K. Raghavachari, J.S. Binkley, C. Gonzalez, R.L. Martin, D.J. Foz, D.J. Defrees, J. Baker, J.J.P. Stewart, J.A. Pople, GAUSSIAN 92/DFT, Gaussian Inc., Pittsburgh, PA, 1993.
[184] J.-D. Marechal, G. Barea, F. Maseras, A. Lleds, L. Mouawad, D. Prahia, J. Comput. Chem. 21 (2000) 282.
[185] P.E. Gill, W. Murray, M.H. Wright, Practical Optimization, Academic Press, New York, 1981.
[186] A.R. Leach, in: K.L. Lipkowitz, D.B. Boyd (Eds.), Reviews in Computational Chemistry, vol. 2, VCH, New York, 1991, p. 1.
[187] D.M. Ferguson, D.J. Raber, J. Am. Chem. Soc. 111 (1989) 4371.
[188] N. Metropolis, A.W. Rosenbluth, M.N. Rosenbluth, A.H. Teller, E. Teller, J. Chem. Phys. 21 (1953) 1087.
[189] T.P. Lybrand, in: K.L. Lipkowitz, D.B. Boyd (Eds.), Reviews in Computational Chemistry, vol. 1, VCH, New York, 1990, p. 295.
[190] M.P. Allen, D.J. Tildesley, Computer Simulation of Liquids, Clarendon, Oxford, UK, 1987.
[191] S. Kirkpatrick, C.D. Gelatt, M.P. Vecchi, Science 220 (1987) 1125.
[192] R. Kaptein, E.R.P. Zuiderweg, R.M. Scheek, R. Boelens, W.F. van Gunsteren, J. Mol. Biol. 182 (1985) 179.
[193] R.E. Bruccoleri, M. Karplus, Biopolymers 29 (1990) 1847.
[194] R. Karaman, Ö. Almarsson, T.C. Bruice, J. Org. Chem. 57 (1992) 1555.
[195] S. Jeon, O. Almarsson, R. Karaman, A. Blasko, T.C. Bruice, Inorg. Chem. 32 (1993) 2562.
[196] F.J. Vergeldt, R.B.M. Koehorst, A. van Hoek, T.J. Schaafsma, J. Phys. Chem. 99 (1995) 4397.
[197] H.N. Fonda, J.V. Gilbert, R.A. Cormier, J.R. Sprague, K. Kamioka, J.S. Connolly, J. Phys. Chem. 97 (1993) 7024.
[198] C. Colominas, L. Eixarch, P. Fors, K. Lang, S. Nonell, J. Teixid, F.R. Trull, J. Chem. Soc. Perkin Trans. 2 (1996) 997.
[199] B. Lament, J. Dobkowski, J.L. Sessler, S.J. Weghorn, J. Waluk, Chem. Eur. J. 5 (1999) 3039.
[200] W.M. Stark, C.J. Hawker, G.J. Hart, A. Philippides, P.M. Petersen, J.D. Lewis, F.J. Leeper, A.R. Battersby, J. Chem. Soc. Perkin Trans. 1 (1993) 2875.
[201] C.J. Hawker, P.M. Petersen, F.J. Leeper, A.R. Battersby, J. Chem. Soc. Perkin Trans. 1 (1998) 1519.
[202] R.P. Bonar-Law, J.K.M. Sanders, J. Chem. Soc. Perkin Trans. I (1996) 3085.
[203] P. Douber-Osguthorpe, V.A. Roberts, D.J. Osguthorpe, J. Wolff, A.T. Genest, A.T. Hagler, Proteins: Struct. Funct. Genet. 4 (1988) 31.
[204] G. Casiraghi, M. Cornia, F. Zanardi, G. Rassu, E. Ragg, R. Bortolini, J. Org. Chem. 59 (1994) 1801.
[205] M. Ravikanth, A. Misra, D. Reddy, T.K. Chandrashekar, J. Chem. Soc. Dalton Trans. (1994) 491.
[206] M. Ravikanth, D. Reddy, T.K. Chandrashekar, Chem. Phys. Lett. 222 (1994) 563.
[207] N.C. Maiti, M. Ravikanath, J. Chem. Soc. Faraday Trans. 91 (1995) 4369.
[208] N.C. Maiti, M. Ravikanath, J. Chem. Soc. Faraday Trans. 92 (1996) 1095.

[209] G. Zheng, M. Shibata, T.J. Dougherty, R.K. Pandey, J. Org. Chem. 65 (2000) 543.
[210] R.J. Abraham, I. Marsden, Tetrahedron 48 (1992) 7489.
[211] L. Griffitths, PhD thesis, University of Liverpool, UK, 1979.
[212] R.J. Abraham, I.S. Haworth, J. Comp.-Aided Mol. Des. 2 (1988) 125.
[213] R.J. Abraham, I.S. Haworth, J. Comp.-Aided Mol. Des. 4 (1990) 283.
[214] R.J. Abraham, G.H. Grant, I.S. Haworth, P.E. Smith, J. Comp.-Aided Mol. Des. 5 (1991) 21.
[215] L. Angelucci, L. DeGioia, P. Fantucci, Gazz. Chim. Ital. 123 (1993) 111.
[216] W.A. Kaplan, K.S. Suslick, R.A. Scott, J. Am. Chem. Soc. 113 (1991) 9824.
[217] M. Abe, T. Kitagawa, Y. Kyogoku, J. Chem. Phys. 69 (1978) 4526.
[218] X.-Y. Li, R.S. Czernuszewicz, J.R. Kincaid, T.G. Spiro, J. Am. Chem. Soc. 111 (1989) 7012.
[219] X.-Y. Li, R.S. Czernuszewicz, J.R. Kincaid, P. Stein, T.G. Spiro, J. Phys. Chem. 94 (1990) 47.
[220] T.D. Brennan, W.R. Scheidt, J.A. Shelnutt, J. Am. Chem. Soc. 110 (1988) 3919.
[221] S.L. Mayo, B.D. Olafson, W.A. Goddard, J. Phys. Chem. 94 (1990) 8897.
[222] L.D. Sparks, W.R. Scheidt, J.A. Shelnutt, Inorg. Chem. 31 (1992) 2191.
[223] J.D. Hobbs, S.A. Majumder, L. Luo, G.A. Sickelsmith, J.M.E. Quirk, C.J. Medforth, K.M. Smith, J.A. Shelnutt, J. Am. Chem. Soc. 116 (1994) 3261.
[224] C.J. Medforth, J.D. Hobbs, M.R. Rodriguez, R.J. Abraham, K.M. Smith, J.A. Shelnutt, Inorg. Chem. 34 (1995) 1333.
[225] K. Yoshizawa, T. Ohta, M. Eda, T. Yamabe, Bull. Chem. Soc. Jpn. 73 (2000) 401.
[226] B. Pispisa, M. Venanzi, L. Stella, A. Palleschi, G. Zanotti, J. Phys. Chem. 103 (1999) 8172.
[227] W.L. Mattice, U.W. Suter, Conformational Theory of Large Molecules, Wiley, New York, 1994.
[228] H.M. Marques, K.L. Brown, J. Mol. Struct. (Theochem.) 340 (1995) 97.
[229] H.M. Marques, C. Warden, M. Monye, M.S. Shongwe, K.L. Brown, Inorg. Chem. 37 (1998) 2578.
[230] D.A. Buckingham, I.E. Maxwell, A.M. Sargeson, M.R. Snow, J. Am. Chem. Soc. 92 (1970) 3617.
[231] M.R. Snow, J. Am. Chem. Soc. 92 (1970) 3610.
[232] L.J. DeHaynes, D.H. Busch, Inorg. Chem. 12 (1973) 1505.
[233] S.R. Niketic, F. Woldbye, Acta Chem. Scand. 27 (1973) 621.
[234] D.A. Buckingham, P.J. Cresswell, R.J. Dellaca, M. Dwyer, G.J. Gainsford, L.G. Marzilli, I.E. Maxwell, W.T. Robinson, A.M. Sargeson, K.R. Turnbull, J. Am. Chem. Soc. 96 (1974) 1713.
[235] D.A. Buckingham, P.J. Cresswell, A.M. Sargeson, Inorg. Chem. 14 (1975) 1485.
[236] T.W. Hambley, C.J. Hawkins, J.A. Palmer, M.R. Snow, Aust. J. Chem. 34 (1981) 45.
[237] J.F. Endicott, G.R. Brubaker, T. Ramasami, K. Kumar, K. Dwarakanath, J. Cassel, D. Johnson, Inorg. Chem. 22 (1983) 3754.
[238] C.L. Schwartz, J.F. Endicott, Inorg. Chem. 29 (1989) 4011.
[239] J.F. Endicott, K. Kumar, C.L. Schwartz, M.W. Perlovic, W.-K. Lin, J. Am. Chem. Soc. 111 (1989) 7411.
[240] Y. Yoshikawa, J. Comput. Chem. 11 (1990) 326.
[241] D.C. Hodgkin, L. Lindsey, R.A. Sparks, K.N. Trueblood, J.G. White, Proc. Roy. Soc. London Ser. A 226 (1962) 494.
[242] J.J.P. Stewart, in: K.L. Lipkowitz, D.B. Boyd (Eds.), Reviews in Computational Chemistry, vol. 1, VCH, New York, 1990, p. 45.
[243] H. Stoeckli-Evans, E. Edmond, D.C. Hodgkin, J. Chem. Soc. Perkin Trans. 2 (1972) 602.
[244] K.L. Brown, D.R. Evans, J.D. Zubkowski, E.J. Valente, Inorg. Chem. 35 (1996) 415.
[245] K.L. Brown, X. Zou, G.-Z. Wu, J.D. Zubkowski, E.J. Valente, Polyhedron 14 (1995) 1621.
[246] A. Bax, L.G. Marzilli, M.F. Summers, J. Am. Chem. Soc. 109 (1987) 566.
[247] K.L. Brown, H.M. Marques, Polyhedron 15 (1996) 2187.
[248] C.J. Medforth, M.O. Senge, T.P. Forsyth, J.D. Hobbs, J.A. Shelnutt, K.M. Smith, Inorg. Chem. 33 (1994) 3865.
[249] P.R. Gerber, K. Gubernator, K. Mhller, Helv. Chim. Acta 71 (1988) 1429.
[250] M.K. Safo, F.A. Walker, A.M. Raitsimring, W.P. Walters, D.P. Dolata, P.G. Debrunner, W.R. Scheidt, J. Am. Chem. Soc. 116 (1994) 7760.
[251] C.J. Medforth, M.O. Senge, K.M. Smith, L.D. Sparks, J.A. Shelnutt, J. Am. Chem. Soc. 114 (1992) 9859.
[252] J.A. Shelnutt, S.A. Majumder, L.D. Sparks, J.D. Hobbs, C.J. Medforth, M.O. Senge, K.M. Smith, M. Miura, L. Luo, J.M.E. Quirk, J. Raman Spectrosc. 23 (1992) 523.
[253] W. Jentzen, E. Unger, X.-Z. Song, S.-L. Jia, I. Turowska-Tyrk, R. Schweitzer-Stenner, W. Dreybrodt, W.R. Scheidt, J.A. Shelnutt, J. Phys. Chem. A 101 (1997) 5789.
[254] L.D. Sparks, C.J. Medforth, M.-S. Park, J.R. Chamberlain, M.R. Ondrias, M.O. Senge, K.M. Smith, J.A. Shelnutt, J. Am. Chem. Soc. 115 (1993) 581.
[255] K.K. Anderson, J.D. Hobbs, L. Luo, K.D. Stanley, J.M.E. Quirk, J.A. Shlenutt, J. Am. Chem. Soc. 115 (1993) 12346.
[256] L.D. Sparks, K.K. Anderson, C.J. Medforth, K.M. Smith, J.A. Shelnutt, Inorg. Chem. 33 (1994) 2297.
[257] X. Song, W. Jentzen, L. Jaquinod, R.G. Khoury, C.J. Medforth, S.-L. Jia, J.-G. Ma, K.M. Smith, J.A. Shelnutt, Inorg. Chem. 37 (1998) 2117.
[258] J.-G. Ma, J. Zhang, R. Franco, S.-L. Jia, I. Moura, J.J.G. Moura, P.M.H. Kroneck, J.A. Shelnutt, Biochemistry 37 (1998) 12431.
[259] J.-G. Ma, M. Laberge, X.-Z. Song, W. Jentzen, S.-L. Jia, J. Zhang, J.M. Vanderkooi, J.A. Shelnutt, Biochemistry 37 (1998) 5118.
[260] J.A. Shelnutt, J. Porphyrins, Phthalocyanines 4 (2000) 386.
[261] J.-P. Gayda, H. Benosman, P. Bertrand, C. More, M. Asso, Eur. J. Biochem. 177 (1988) 199.
[262] G. Palmer, Biochem. Soc. Trans. 13 (1985) 548.
[263] I. Moura, M. Teixeira, J. LeGall, J.J.G. Moura, B.H. Huynh, Eur. J. Biochem. 176 (1988) 365.
[264] O.Q. Munro, J.A. Serth-Guzzo, I. Turowska-Tyrk, K. Mohanrao, T.K. Shokhireva, F.A. Walker, P.G. Debrunner, W.R. Scheidt, J. Am. Chem. Soc. 121 (1999) 11144.
[265] H.M. Marques, K. Voster, T.J. Egan, J. Inorg. Biochem. 64 (1996) 7.
[266] T.J. Egan, Exp. Opin. Ther. Patents 11 (2001) 1.
[267] O.Q. Munro, P.S. Madlala, R.A.F. Warby, T.B. Seda, G. Hearne, Inorg. Chem. 38 (1999) 4724.
[268] K. Momot, F.A. Walker, J. Phys. Chem. A 101 (1997) 2787.
[269] C.J. Medforth, C.M. Muzzi, K.M. Shea, K.M. Smith, R.J. Abraham, S. Jia, J.A. Shelnutt, J. Chem. Soc. Perkin Trans. 2 (1997) 833.
[270] C.J. Medforth, C.M. Muzzi, K.M. Smith, R.J. Abraham, J.D. Hobbs, J.A. Shelnutt, J. Chem. Soc. Chem. Commun. (1994) 1843.
[271] M.W. Renner, K.M. Barkigia, D. Melamed, K.M. Smith, J. Fajer, Inorg. Chem. 35 (1996) 5120.
[272] S.-L. Jia, W. Jentzen, M. Shang, X.-Z. Song, J.-G. Ma, W.R. Scheidt, J.A. Shelnutt, Inorg. Chem. 37 (1988) 4402.
[273] R.J. Abraham, G.R. Bedford, D. McNeill, B. Wright, Org. Magn. Res. 14 (1980) 418.
[274] R.D. Hancock, J. Chem. Soc. Dalton Trans. (1986) 2505.
[275] E.B. Fleischer, Acc. Chem. Res. 3 (1970) 105.

[276] M.F. Perutz, Proc. Roy. Soc. London. Ser B. 173 (1969) 113.
[277] L.D. Sparks, J.R. Chamberlain, P. Hsu, M.R. Ondrias, B.A. Swanson, P.R. Ortiz de Montellano, J.R. Shelnutt, Inorg. Chem. 32 (1993) 3153.
[278] E. Monzani, L. Linati, L. Casella, L. De Gioia, M. Favretto, M. Gullotti, F. Chillemi, Inorg. Chim. Acta 273 (1998) 339.
[279] B. Cheng, J.D. Hobbs, P.G. Debrunner, J. Erlebacher, J.A. Shelnutt, W.R. Scheidt, Inorg. Chem. 34 (1995) 102.
[280] X. Song, M. Miura, X. Xu, K.K. Taylor, S.A. Majumder, J.D. Hobbs, J. Cesaerano, J.A. Shelnutt, Langmuir 12 (1996) 2019.
[281] H.M. Marques, in: R. Banerjee (Ed.), Chemistry and Biochemistry of B12, Wiley, New York, 1999, p. 289.
[282] H.M. Marques, K.L. Brown, Inorg. Chem. 34 (1995) 3733.
[283] Y. Toraya, R.L. Blakely, Biochemistry 12 (1973) 24.
[284] S.M. Chemaly, J.M. Pratt, J. Chem. Soc. Dalton Trans. (1980) 2259.
[285] J.M. Pratt, J. Mol. Catal. 23 (1984) 187.
[286] Y. Toraya, T. Matsumoto, M. Ichikawa, Y. Itah, T. Sugawara, Y. Mizuno, J. Biol. Chem. 261 (1986) 9289.
[287] B.M. Babior, in: B. Zagalak, W. Friedrich (Eds.), Vitamin B12, Walter de Gruyter, New York, 1979, p. 461.
[288] J.H. Grate, G.N. Schrauzer, J. Am. Chem. Soc. 101 (1979) 6401.
[289] G.N. Schrauzer, J.H. Grate, J. Am. Chem. Soc. 103 (1981) 541.
[290] J. Halpern, Science 227 (1985) 869.
[291] K.L. Brown, H.M. Marques, J. Inorg. Biochem. 83 (2001) 121.
[292] A.D. Bacon, M.C. Zerner, Theor. Chim. Acta 53 (1979) 21.
[293] W.P. Anderson, W.D. Edwards, M.C. Zerner, Inorg. Chem. 25 (1986) 2728.
[294] K.L. Brown, H. Brooks, Inorg. Chem. 30 (1991) 3420.
[295] K.L. Brown, H.B. Brooks, D. Behnke, D.W. Jacobsen, J. Biol. Chem. 226 (1991) 6737.
[296] K.L. Brown, X. Zou, D.R. Evans, Inorg. Chem. 33 (1994) 5713.
[297] K.L. Brown, S. Cheng, H.M. Marques, Inorg. Chem. 34 (1995) 3038.
[298] K.L. Brown, D.R. Evans, S. Cheng, H.M. Marques, J.D. Zubkowski, E.J. Valente, Recent Res. Dev. Inorg. Chem. 1 (1998) 1.
[299] K.L. Brown, S. Cheng, H.M. Marques, Polyhedron 17 (1998) 2213.
[300] K.L. Brown, S. Cheng, X. Zou, G. Chen, E.J. Valente, J.D. Zubkowski, H.M. Marques, Biochemistry 37 (1998) 9704.
[301] W.F. Gunsteren, H.J.C. Berendsen, Angew. Chem. Intl. Ed. Engl. 29 (1990) 992.
[302] M. Karplus, G.A. Petsko, Nature 347 (1990) 631.
[303] E. Saiz, M.P. Tarazona, J. Chem. Educ. 74 (1997) 1350.
[304] G.M. Clore, A.T. Brünger, M. Karplus, A.M. Gronenborn, J. Mol. Biol. 191 (1986) 523.
[305] K.L. Brown, X. Zou, H.M. Marques, J. Mol. Struct. (Theochem.) 453 (1998) 209.
[306] J. Ryckaert, G. Ciccotti, H. Berendsen, J. Comput. Phys. 23 (1977) 327.
[307] P.A. Kollman, P.D.J. Grottenhuis, M.A. Lopez, Pure Appl. Chem. 61 (1989) 593.
[308] M.A. Lopez, P.A. Kollman, J. Am. Chem. Soc. 111 (1989) 6212.
[309] M.J.S. Dewar, E.G. Zoebisch, E.F. Healy, J.J.P. Stewart, J. Am. Chem. Soc. 107 (1985) 3902.
[310] M.J.S. Dewar, J.K.M. Dieter, J. Am. Chem. Soc. 108 (1986) 8075.
[311] M. Frank, K. Peraus, H.A. Staab, J. Mol. Model. 2 (1996) 383.
[312] T. Sato, K. Sugao, Y. Oumi, R. Vetrivel, M. Chatterjee, A. Chatterjee, M. Kubo, A. Stirling, A. Fahmi, A. Miyamoto, Appl. Surf. Sci. 119 (1997) 346.
[313] K. Kawamura, in: F. Yonezawa (Ed.), Molecular Dynamics Simulations, Springer, Berlin, 1992, p. 88.
[314] J. Aron, D.A. Baldwin, H.M. Marques, J.M. Pratt, P.A. Adams, J. Inorg. Biochem. 27 (1986) 227.
[315] O.Q. Munro, H.M. Marques, Inorg. Chem. 35 (1996) 3752.
[316] P.A. Adams, D.A. Baldwin, H.M. Marques, in: R.A. Scott, A.G. Mauk (Eds.), Cytochrome *c*: A Multidisciplinary Approach, University Science Books, Sausalito, CA, 1996, pp. 635–692.
[317] H.M. Marques, M.S. Shongwe, O.Q. Munro, T.J. Egan, S. Afr. J. Chem. 50 (1997) 166.
[318] G. Ranghino, G. Antonini, P. Fantucci, Isr. J. Chem. 34 (1994) 239.
[319] H.M. Marques, C.B. Perry, J. Inorg. Biochem. 75 (1999) 281.
[320] S. Melchionna, M. Barteri, G. Ciccotti, J. Comput.-Aided Mat. Des. 2 (1995) 9.
[321] W.F. van Gunsteren, H.J.C. Berendsen, Groningen Molecular Simulation (GROMOS) Library, Groningen, Netherlands, 1987.
[322] S. Melchionna, M. Barteri, G. Ciccotti, J. Phys. Chem. 100 (1996) 19241.
[323] E.R. Henry, M. Levitt, W.A. Eaton, Proc. Natl. Acad. Sci. USA 82 (1985) 2034.
[324] M. Levitt, J. Mol. Biol. 168 (1983) 595.
[325] W. Nowak, J. Mol. Struct. (Theochem.) 398–399 (1997) 537.
[326] R.A. Elber, A. Roitber, C. Simmerling, R. Goldstein, H. Li, G. Verkhivker, C. Keasar, J. Zhang, A. Ulitsky, Comput. Phys. Commun. 91 (1995) 159.
[327] J. Czarnecka, Masters thesis, Torun, Poland, 1996.
[328] O. Edholm, P.I. Ohlsson, M.L. Smith, J. Paul, Chem. Phys. Lett. 291 (1998) 501.
[329] P. Jewsbury, T. Kitagawa, Biophys. J. 67 (1994) 2236.
[330] K.G. Welinder, Eur. J. Biochem. 151 (1985) 497.
[331] I.M.C. Rietjens, A.M. Osman, C. Veeger, O. Zakharieva, J. Antony, M. Grodzicki, A.X. Trautwein, J. Biol. Inorg. Chem. 1 (1996) 372.
[332] S.K. Chapman, S. Daff, A.W. Munro, Struct. Bonding (Berlin) 88 (1997) 39.
[333] I. Fita, M.G. Rossmann, J. Mol. Biol. 185 (1985) 21.
[334] T.L. Poulos, S.T. Freer, R.A. Alden, S.L. Edwards, U. Skogland, K. Takio, B. Eriksson, N. Xuong, T. Yonetani, J. Kraut, J. Biol. Chem. 255 (1980) 575.
[335] B.C. Finzel, T.L. Poulos, J. Kraut, J. Biol. Chem. 259 (1984) 13027.
[336] W.R. Patterson, T.L. Poulos, Biochemistry 34 (1995) 4331.
[337] J.F.W. Petersen, A. Kadziola, S. Larsen, FEBS Lett. 339 (1994) 291.
[338] N. Kunishima, K. Fukuyama, H. Matsubara, H. Hatanaka, Y. Shibano, T. Amachi, J. Mol. Biol. 235 (1994) 331.
[339] K. Piontek, T. Glumoff, K. Winterhalter, FEBS Lett. 315 (1993) 119.
[340] T.L. Poulos, S.L. Edwards, H. Wariishi, M.H. Gold, J. Biol. Chem. 268 (1993) 4429.
[341] S.L. Edwards, R. Raag, H. Wariishi, M.H. Gold, T.L. Poulos, Proc. Natl. Acad. Sci. USA 90 (1993) 750.
[342] D.J. Schuller, N. Ban, R.B. van Huystee, A. McPhirson, T.L. Poulos, Structure (London) 4 (1996) 311.
[343] M. Gajhede, D.J. Schuller, A. Henriksen, A.T. Smith, T.L. Poulos, Nat. Struct. Biol. 4 (1997) 1032.
[344] M. Sundaramoorthy, K. Kishi, M.H. Gold, T.L. Poulos, J. Biol. Chem. 269 (1994) 32759.
[345] H. Pelletier, J. Kraut, Science 258 (1992) 1748.
[346] J.E. Erman, L.B. Vitello, M.A. Miller, A. Shaw, K.A. Broen, J. Kraut, Biochemistry 32 (1993) 9798.
[347] L.B. Vitello, J.E. Erman, M.A. Miller, J. Wang, J. Kraut, Biochemistry 32 (1993) 9807.
[348] S. Ogawa, Y. Shiro, I. Morishima, Biochem. Biophys. Res. Commun. 90 (1979) 674.

[349] I. Morishima, M. Kurono, Y. Shiro, J. Biol. Chem. 261 (1986) 9391.
[350] K.R. Barber, M.J. Rodriguez Maranon, G.S. Shaw, R.B. van Huystee, Eur. J. Biochem. 232 (1995) 825.
[351] L. Banci, P. Carloni, G. Gori Savellini, Biochemistry 33 (1994) 12356.
[352] L. Banci, P. Carloni, A. Diaz, G. Gori Savellini, J. Biol. Inorg. Chem. 1 (1996a) 264.
[353] W. Jorgensen, J. Chandrasekar, J. Madura, R. Impey, M. Klein, J. Chem. Phys. 79 (1983) 926.
[354] P. Argos, F. Mathews, J. Biol. Chem. 250 (1975) 747.
[355] H.H. Ruf, P. Wende, V. Ullrich, J. Inorg. Biochem. 11 (1979) 189.
[356] J.H. Dawson, L.A. Andersson, M. Sono, J. Biol. Chem. 257 (1982) 3606.
[357] R.A. Scott, A.G. Mauk (Eds.), Cytochrome *c*: A Multidisciplinary Approach, University Science Books, Sausalito, CA, 1996.
[358] G.R. Moore, G.W. Pettigrew (Eds.), Cytochrome *c*: Evolutionary, Structural and Physicochemical Aspects, Springer-Verlag, Berlin, 1990.
[359] C. Wong, C. Zheng, J. Shen, J. McCammon, P. Wolneys, J. Phys. Chem. 97 (1993) 3100.
[360] A. Churg, R. Weiss, A. Warshel, T. Takano, J. Phys. Chem. 87 (1983) 1683.
[361] A. Churg, A. Warshel, Biochemistry 25 (1986) 1675.
[362] G.D. Brayer, M.E.P. Murphy, in: R.A. Scott, A.G. Mauk (Eds.), Cytochrome *c*: A Multidisciplinary Approach, University Science Books, Sausalito, CA, 1996.
[363] G.W. Bushnell, G.V. Louie, G.D. Brayer, J. Mol. Biol. 214 (1990) 585.
[364] A.M. Berghuis, G.D. Brayer, J. Mol. Biol. 223 (1992) 959.
[365] A.M. Berghuis, J.G. Guillemette, G. McLendon, F. Sherman, M. Smith, G.D. Brayer, J. Mol. Biol. 236 (1994) 786.
[366] P.X. Qi, J.L. Urbauer, E.J. Fuentes, M.F. Leopold, A.J. Wand, Nat. Struct. Biol. 1 (1994) 378.
[367] J.A. Cowan, Inorganic Biochemistry—An Introduction, 2nd ed., Wiley-VCH, New York, 1997, p. 334.
[368] T.L. Poulos, B.C. Finzel, A.J. Howard, Biochemistry 25 (1986) 5314.
[369] T.L. Poulos, B.C. Finzel, A.J. Howard, J. Mol. Biol. 195 (1987) 687.
[370] M.D. Paulsen, R.L. Ornstein, Proteins: Struct. Funct. Genet. 11 (1991) 184.
[371] D.A. Giammona, PhD Thesis, University of California, Davis, CA, 1986.
[372] M.D. Paulsen, R.L. Ornstein, Proteins: Struct. Funct. Genetics 21 (1995) 237.
[373] K.G. Ravichandran, S.S. Boddupalli, C.A. Hasemann, J.A. Peterson, J. Deisenhofer, Science 261 (1993) 731.
[374] S.K. Lüdemann, O. Carugo, R.C. Wade, J. Mol. Model. 3 (1997) 369.
[375] Y. Chang, O.B. Stiffelman, G.H. Loew, Biochimie 78 (1996) 771.
[376] L. Holm, C. Sander, J. Mol. Biol. 218 (1991) 183.
[377] M.J. Sippl, J. Comput.-Aided Mol. Des. 7 (1993) 473.
[378] D. Harris, G.H. Loew, J. Am. Chem. Soc. 117 (1995) 2738.
[379] G.D. Szklarz, J.R. Halpert, J. Comput.-Aided Mol. Des. 11 (1997) 265.
[380] M.D. Paulsen, J.I. Manchester, R.L. Orenstein, Methods Enzymol. 272 (1996) 347.
[381] H.M. Marques, R.P. Hicks, K.L. Brown, J. Chem. Soc. Chem. Commun. (1996) 1427.
[382] H.M. Marques, X. Zou, K.L. Brown, J. Mol. Struct. 520 (2000) 75.
[383] M. Rossi, J.P. Glusker, L. Randaccio, L. Marzilli, J. Am. Chem. Soc. 107 (1985) 1729.
[384] J.P. Bouquiere, J.L. Finney, M.S. Lehmann, P.F. Lindley, H.F.J. Savage, Acta Crystallogr. Sect. B 49 (1993) 79.
[385] R.J. Blau, J.A. Espenson, J. Am. Chem. Soc. 107 (1985) 3530.
[386] B.P. Hay, R.G. Finke, J. Am. Chem. Soc. 109 (1987) 8012.
[387] S.-H. Kim, H.L. Chen, N. Feilchenfeld, J. Halpern, J. Am. Chem. Soc. 110 (1988) 3120.
[388] T. Simonson, D. Perahia, J. Am. Chem. Soc. 117 (1995) 7987.
[389] F.S. Mathews, Prog. Biophys. Mol. Biol. 45 (1985) 1.
[390] E.M. Storch, V. Daggett, Biochemistry 35 (1996) 11596.
[391] M. Levitt, J. Mol. Biol. 181 (1989) 423.
[392] M. Levitt, M. Hirshberg, R. Sharon, V. Daggett, Comput. Phys. Commun. 91 (1995) 215.
[393] M. Levitt, ENCAD—Energy Calculation and Dynamics, Molecular Applications Group, Stanford, CA, 1990.